

# Counterpropagating optical beams and solitons

Milan S. Petrović,<sup>1,2</sup> Milivoj R. Belić,<sup>1</sup> Cornelia Denz,<sup>3</sup> and Yuri S. Kivshar<sup>4</sup>

<sup>1</sup>Texas A&M University at Qatar, P. O. Box 23874, Doha, Qatar

<sup>2</sup>Institute of Physics, P. O. Box 57, 11001 Belgrade, Serbia

<sup>3</sup>Institut für Angewandte Physik und Center for Nonlinear Science (CeNoS),  
Westfälische Wilhelms-Universität, D-48149 Münster, Germany

<sup>4</sup>Nonlinear Physics Center, Research School of Physics and Engineering,  
Australian National University, Canberra ACT 0200, Australia

Physics of counterpropagating optical beams and spatial optical solitons is reviewed, including the formation of stationary states and spatiotemporal instabilities. First, several models describing the evolution and interactions between optical beams and spatial solitons are discussed, that propagate in opposite directions in nonlinear media. It is shown that coherent collisions between counterpropagating beams give rise to an interesting focusing mechanism resulting from the interference between the beams, and that interactions between such beams are insensitive to the relative phase between them. Second, recent experimental observations of the counterpropagation effects and instabilities in waveguides and bulk geometries, as well as in one- and two-dimensional photonic lattices, are discussed. A variety of different generalizations of this concept are summarized, including the counterpropagating beams of complex structures, such as multipole beams and optical vortices, as well as the beams in different media, such as photorefractive materials and liquid crystals.

PACS numbers: 42.65.Jx, 42.65.Tg, 42.65.Sf, 42.70.Mp.

## I. INTRODUCTION

One of the simplest processes in nonlinear (NL) optics leading to a variety of complex NL physics phenomena is the mutual interaction of two counterpropagating (CP) optical beams in a NL medium, capable of nonlinearly changing the refractive index of the medium. The underlying geometry is conceptually very simple (see Fig. 1): two beams enter a finite NL medium from the opposite sides and, when they overlap by their evanescent fields, the beams start interacting via the mutual NL change of the optical refractive index. A configuration of two waves interacting in a NL material is one of the most frequent ones in laser physics and wave mixing experiments. Numerous concepts in NL optics, such as phase conjugation, Bragg reflection by volume gratings, wave-mixing in photorefractives, *etc.*, are based on this simple geometry. Nevertheless, this simple geometry can give rise to an extremely complicated and sometimes counterintuitive dynamical behavior, including both mutual beam self-trapping and the formation of stationary states, as well as complex spatiotemporal (ST) instabilities [1]. It is for these reasons that CP beam configurations have achieved a paradigmatic role in NL physics of optical systems.

Instabilities and chaos are typically expected to appear in NL optical systems that feature coupling as well as feedback as necessary ingredients. Therefore, CP waves were first studied in more complex systems than the configuration described above, foremost in NL optical resonators. CP beams in Fabry-Perot resonators have been studied by Ikeda *et al.* [2, 3]. They demonstrated that a ring resonator with Kerr nonlinearity undergoes a series of bifurcations, as the incident power is increased, leading to chaos and "optical turbulence". Similar ST

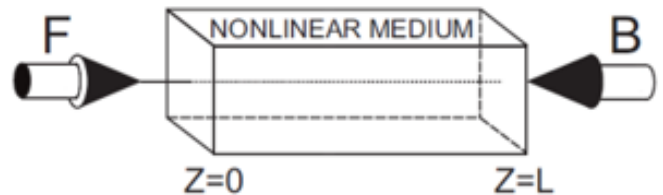


FIG. 1: General schematic of two counterpropagating waves interacting in a finite-length nonlinear medium.

instabilities were observed later in simpler configurations with only a single mirror, known as the single feedback systems, especially in the ones exhibiting saturable nonlinearities, such as atomic vapors [4, 5, 6, 7], liquid crystals [8], and photorefractive (PR) media [9]. For example, instabilities in the polarizations of CP beams were observed in atomic sodium vapor [4, 5], when for higher intensities the polarization first varies periodically and then the system dynamics becomes chaotic (see also Ref. [10]). Silberberg and Bar Joseph [1] were the first to demonstrate that even without an external feedback, instabilities and chaos can be observed in the simplest geometry shown in Fig. 1. In their configuration, the origin of instability was the combined action of gain due to four-wave mixing and distributed feedback due to scattering from the grating formed by the interference of the incident laser beams. This discovery opened the possibility of considering CP beam configuration as a fundamental configuration to investigate NL physics phenomena in optics.

Such a possibility was backed up by many subsequent observations, showing that when taking into account transverse extent of the interacting beams, an even more complicated behavior can emerge, including oscil-

latory transverse instabilities [11, 12] and pattern formation [13, 14, 15] that require neither cavity nor finite response time. Sometimes, these instabilities could be associated with interesting transverse structures, such as polarization domain walls [16, 17], supported by the mixing of two CP laser beams in a NL isotropic dielectric medium. Since transverse instabilities of CP optical beams lead to pattern generation, a natural question arises in CP systems: which patterns may survive in this geometry. Among the various pattern classes especially singular structures and localized states gained interest, owing to their strong NL nature most often associated with subcritical bifurcations [18].

In addition to these localized states or dissipative (cavity) solitons, which are stabilized due to the common action of gain, loss, nonlinearity and diffraction, the propagation and self-action of a single beam in a NL medium is also known to generate spatial solitons [19]. Therefore, a natural extension was to study the propagation and interaction of CP spatial solitons and their generalizations, and to build a connection between these solitons and the feedback or cavity solitons, thereby attempting to answer fundamental questions about the nature and relations of propagating and dissipative solitons in media with NL optical refractive index.

Collisions between solitons are perhaps the most fascinating feature of soliton phenomena, because the interacting self-trapped wave packets exhibit many particle-like features [20]. Solitons that propagate in the opposite direction enable a natural mechanism of soliton collisions, resulting from the strong interaction of the two beams. The CP solitons interfere and give rise to an effective grating. For copropagating solitons, the grating is periodic in the transverse direction, with a period much greater than the optical wavelength; thus the interacting solitons go through very few grating periods. For CP collisions in contrast the grating is in the propagation direction, hence the interacting solitons go through many periods. Consequently, the interaction in the CP scheme is strongly affected by the mutual Bragg scattering. Moreover, in the case of incoherent interacting beams, the CP scheme also allows for strong interaction, due to cross-coupling of the beams via the common refractive index structure that is not present in the copropagating case.

Owing to these reasons, CP solitons assumed a paradigmatic role in the physics of NL optics: mutual self-trapping of two CP optical beams was shown to lead to the formation of a novel type of vector (or bimodal) solitons [21, 22], for both coherent and incoherent interactions. A more detailed analysis [23] revealed that these CP solitons may display a variety of instabilities, accompanied by nontrivial temporal and spatial dynamics, leading to many subsequent studies devoted to this fundamentally new subject.

This paper aims to review the fundamental physics of CP optical beams and spatial optical solitons, and their paradigmatic role in NL optics, including the whole range of NL physics phenomena, from the formation of station-

ary states up to ST instabilities. It summarizes a number of recent important results for the evolution and interaction of optical beams and spatial solitons that propagate in opposite directions, thereby emphasizing their general importance for NL physics.

The paper is organized as follows. In Sec. 2 we present the derivation of a one-dimensional (1D) model for the beam propagation in a planar structure in PR NL crystals, and then apply it to the analysis of mutual self-trapping and modulational instabilities (MIs) of CP beams and spatial solitons. Section 3 is devoted to the analysis of 2D models, where we discuss nontrivial rotational beam dynamics and the transverse pattern formation. In Sec. 4 we present the key experimental results for both one- and two-dimensional geometries. The more special case of solitons counterpropagating in optical lattices is discussed in Sec. 5, where we summarize both theoretical and experimental results. Section 6 is devoted to the discussion of various generalizations of the concept of beam counterpropagation, including the counterpropagation of multipoles and vortex optical beams, as well as the beam interaction in liquid crystals. Finally, Sec. 7 concludes the paper.

## II. ONE-DIMENSIONAL SYSTEMS

### A. Theoretical models and background

Early theoretical descriptions of CP self-trapped beams, in one transverse dimension and steady-state, were given in [22], where bimodal CP solitons in Kerr media have been treated, and in [21], where collisions of solitons propagating in opposite directions, in both Kerr and local PR media, have been addressed. Following a more general exposition [23], we present here the basic equations for the propagation and interactions of CP beams in saturable PR media. The temporal behavior of CP self-trapped beams is included in the equations by a time-relaxation procedure for the formation of space charge field and refractive index modulation in the crystal.

We consider two CP light beams in a PR crystal, in the paraxial approximation, under conditions suitable for the formation of screening solitons. The optical field is given as the sum of CP waves  $F \exp(ikz + i\omega t) + B \exp(-ikz + i\omega t)$ ,  $k$  being the wave vector in the medium,  $F$  and  $B$  are the slowly varying envelopes of the beams. The light intensity  $I$  is measured in units of the background light intensity, also necessary for the generation of solitons. After averaging in time on the scale of the response time  $\tau_0$  of the PR crystal, the total intensity is given by

$$1 + I = (1 + I_0) \{1 + \varepsilon [m \exp(2ikz) + c.c.] / 2\}, \quad (1)$$

where  $I_0 = |F|^2 + |B|^2$ ,  $m = 2FB^*/(1 + I_0)$  is the modulation depth, and *c.c.* stands for complex conjugation.

Here the parameter  $\varepsilon$  measures the degree of temporal coherence of the beams relative to the crystal relaxation time. For  $\varepsilon = 0$ , *i.e.*, when the relative phase of the beams varies much faster than  $\tau_0$ , the beams are effectively incoherent. In the opposite case  $\varepsilon = 1$ , the intensity distribution contains an interference term that is periodically modulated in the direction of propagation  $z$ , chosen to be perpendicular to the  $c$  axis of the crystal, which is also the  $x$  axis of the coordinate system. Beams are polarized in the  $x$  direction, and the external electric field  $E_e$ , necessary for the formation of self-trapped beams, also points in the  $x$  direction. The electric field in the crystal couples to the electrooptic tensor, giving rise to a change in the index of refraction of the form  $\Delta n = -n_0^3 r_{eff} E/2$ , where  $n_0$  is the unperturbed index,  $r_{eff}$  is the effective component of the electro-optic tensor, and  $E$  is the  $x$  component of the total electric field. It consists of the external field and the space charge field  $E_{sc}$  generated in the crystal,  $E = E_e + E_{sc}$ .

The intensity modulates the space charge field, which is represented in the normalized form

$$E_{sc}/E_e = E_0 + \frac{1}{2} [E_1 \exp(2ikz) + c.c.], \quad (2)$$

where  $E_0$  is the homogeneous part of the  $x$  component of the space charge field, and  $E_1(x, z)$  is the slowly varying part of the space charge field, proportional to  $\varepsilon$ . It is  $E_0$  that screens the external field, and  $E_1$  is the result of the interference pattern along the  $z$  direction.

In the isotropic approach, one assumes a local approximation to the space charge field, and looks for a solution with the saturable nonlinearity  $E = E_e/(1 + I)$ . Substituting Eqs. (1) and (2) in this expression, and neglecting higher harmonics and terms quadratic in  $m$ , the steady-state solutions  $E_0 = -I_0/(1 + I_0)$  and  $E_1 = -\varepsilon m/(1 + I_0)$  are obtained. The temporal evolution of the space charge field is introduced by assuming relaxation-type dynamics

$$\tau \partial_t E_0 + E_0 = -\frac{I_0}{1 + I_0}, \quad (3a)$$

$$\tau \partial_t E_1 + E_1 = -\frac{\varepsilon m}{1 + I_0}, \quad (3b)$$

where the relaxation time of the crystal  $\tau$  is inversely proportional to the total intensity  $\tau = \tau_0/(1 + I)$ , *i.e.*, the illuminated regions in the crystal react faster. The assumed dynamics is that the space charge field builds up towards the steady state, which depends on the light distribution, which in turn is slaved to the slow change of the space charge field. As it will be seen later, this assumption does not preclude a more complicated dynamical behavior.

Selecting synchronous terms in the NL paraxial wave equation, leads to the propagation equations in the form:

$$i\partial_z F + \partial_x^2 F = \Gamma [E_0 F + E_1 B/2], \quad (4a)$$

$$-i\partial_z B + \partial_x^2 B = \Gamma [E_0 B + E_1^* F/2], \quad (4b)$$

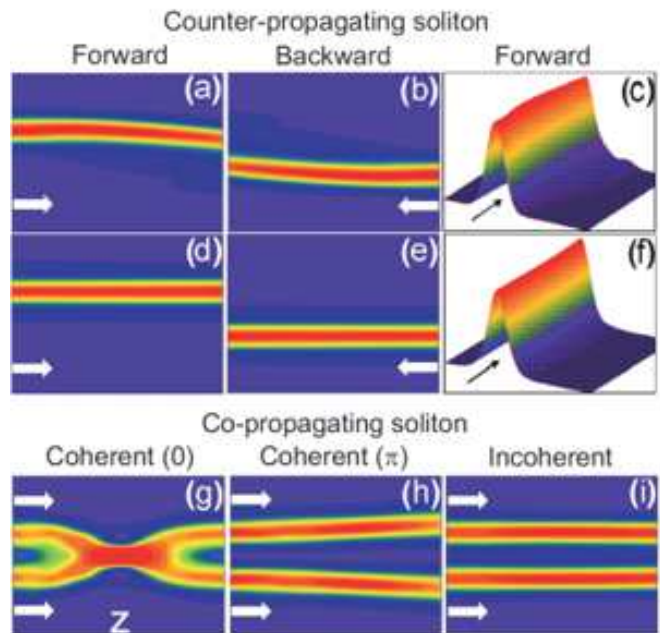


FIG. 2: (a)-(c) Coherent interactions between the CP (a),(c) forward and (b) backward solitons. (d)-(f) Incoherent interactions between the CP (d),(f) forward and (e) backward solitons. For comparison, interactions between coherent in-phase (g) and  $\pi$  out of phase (h), and incoherent (i) copropagating solitons. The plots show intensities. The arrow indicates the propagation direction of each beam. The propagation distance is  $2.5 L_D$ . Adopted from [21].

where the parameter  $\Gamma = (kn_0 x_0)^2 r_{eff} E_e$  is the dimensionless coupling strength, and the scaling  $x \rightarrow x/x_0$ ,  $z \rightarrow z/L_D$ ,  $(F, B) \rightarrow (F, B) \exp(-i\Gamma z)$  is used. Here  $x_0$  is the typical beam waist and  $L_D = 2kx_0^2$  is the diffraction length. Propagation equations are solved numerically, concurrently with the temporal equations. The numerical procedure consists in solving Eqs. (3) for the components of the space charge field, with the light fields obtained at every step as guided modes of the induced common waveguide.

## B. Counterpropagating solitons

We consider first the interactions in a configuration where the two CP beams are launched parallel to each other, but with a transverse spacing between them [21]. The parameters are chosen such that the formation of spatial solitons is preferred. The coherent interaction between these parallel CP beams is shown in Figs. 2(a)-2(c). Figures 2(d)-2(f) show an incoherent interaction between the same beams. For comparison, the same beams in copropagating scheme are simulated in Figs. 2(g)-2(i). Figure 2(g) [2(h)] shows a coherent interaction in which the relative phase between the launched beams is 0 [ $\pi$ ]. Figure 2(i) shows an incoherent interaction. Clearly, the outcome of the interaction between the beams in the CP

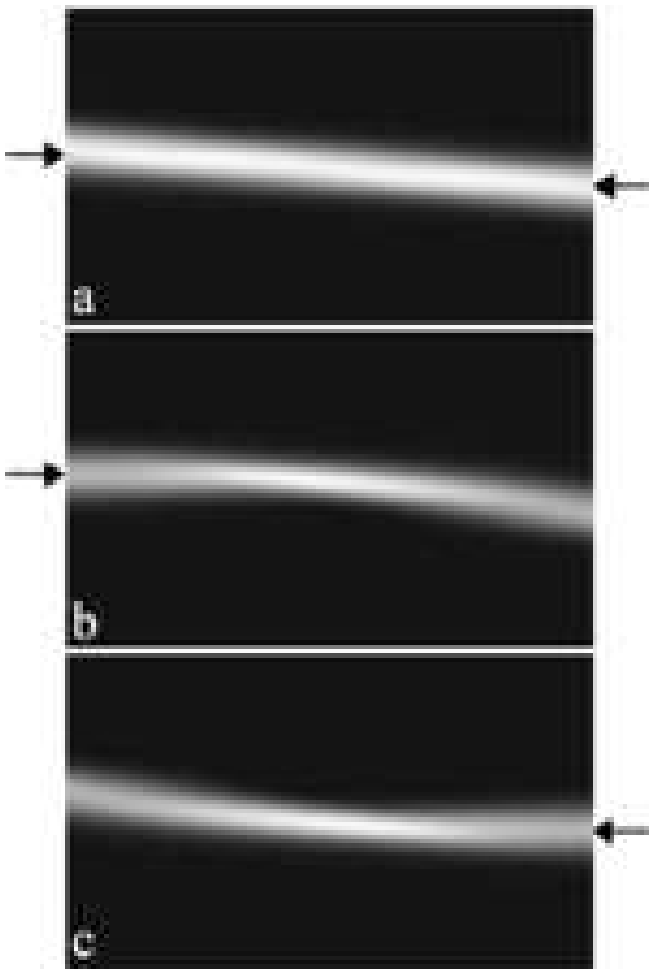


FIG. 3: Bidirectional waveguide. (a) Total intensity distribution; (b) right-propagating and (c) left-propagating beams. Parameters:  $\varepsilon = 1$ ,  $\Gamma = 5$ , initial peak intensities  $|F_0|^2 = |B_L|^2 = 1$ . The size of data windows is 10 beam diameters transversely by 2 diffraction lengths longitudinally. Reprinted from [23].

scheme is very different from the one in the copropagating scheme, in both the coherent and incoherent cases. First, in the copropagating scheme, the mutual force between the solitons is proportional to the relative phase between them, hence the interaction can be attractive [Fig. 2(g)] or repulsive [Fig. 2(h)]. In contrast, in the CP case the relative phase oscillates on a scale much shorter than the soliton period, thus the relative phase does not play any role.

The second major difference between the counter- and copropagating cases has to do with the radiation. The coherent interaction in the CP scheme radiates [Figs. 2(a) and 2(b)], which again proves that this system is nonintegrable. On the other hand, the incoherent interaction between the CP solitons does not radiate much [Figs. 2(d)-2(f)]. Finally, one can see that a portion of the forward beam couples into the region where the backward beam is propagating. In the incoherent interaction, the

forward beam gradually tunnels into the backward soliton region, hence the forward intensity at the backward soliton region increases monotonically [Fig. 2(f)]. This behavior represents an example of directional coupling or resonant tunneling. For coherent interactions the dynamics are more complex, as the intensity coupled from the forward beam to the region "under" the backward beam oscillates [see the sidebands in Fig. 2(c)], and, in contradistinction to the incoherent case, light does not accumulate in the "sidebands."

Head-on collision of the beams with initial soliton profiles, after temporal relaxation to a steady state, results in the formation of a CP soliton [23]. Shooting initial beams with arbitrary parameters generally leads to the  $z$  dependent or nonstationary character of the beam propagation. In some domain of the initial parameters, for example with the relative angle of beam scattering  $\theta$  close to  $\pi$  and small initial transverse offset, the time-relaxation procedure converges to the stationary in time structures, which are identified as the steady-state self-trapped waveguides, or as bent CP solitons. The formation of a single bidirectional waveguide is shown in Fig. 3. Two coherent Gaussian beams are launched at different lateral positions perpendicular to the crystal edges,  $\theta = \pi$ . Both beams diffract initially, until the space charge field is developed in time, to form the waveguide induced by the total light intensity, Fig. 3(a). This induced waveguide traps both beams, Figs. 3(b) and 3(c). When the initial transverse separation is four or more beam diameters, the beams hardly feel the presence of each other, and focus into individual solitons. For the separation of two beam diameters, the interaction is strong enough for the beams to form a joint waveguiding structure, as is shown in Fig. 3.

### C. Splitup transition

Consideration of a wider region of control parameters leads to a more complex picture. To capture the transition from a CP soliton to a waveguide more clearly, the head-on collision of two identical Gaussian beams was considered in [24, 25]. In the absence of the other, each beam focuses into a soliton. The situation when they are both present, and when the coupling constant  $\Gamma$  and the crystal length  $L$  are both varied, is displayed in Fig. 4. It is seen that in the plane  $(L, \Gamma)$  of control parameters there exists a critical curve below which the stable CP solitons exist (the first curve in Fig. 4). At that critical curve a new type of solution appears, after a symmetry breaking transition, in which the two components no longer overlap, but split and cross each other. We term this phenomenon the splitup transition [23]. A few examples are depicted in the insets in Fig. 4. As the beams split, a portion of each beam remains guided by the other, forming bidirectional waveguides. Both the solitons and the waveguides are steady-state solutions. As one moves away from the first critical curve, into the

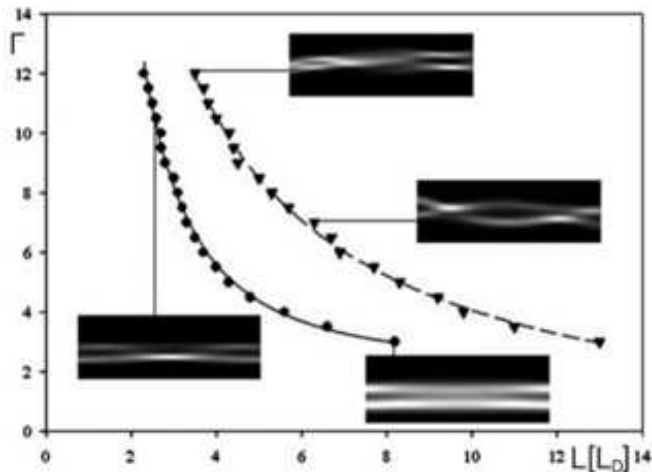


FIG. 4: Critical curves in the parameter plane for the existence of stable CP solitons, bidirectional waveguides and unstable solutions. Below the first curve CP solitons exist, between the curves bidirectional waveguides appear. At and above the second curve unstable solutions emerge. Insets depict typical beam intensity distributions in the  $(x, z)$  plane at the points indicated. The points are numerically determined, the curves are inverse power polynomial fits. Reprinted from [25].

region of high couplings and long crystals, a new critical curve is approached, where the steady-state waveguides lose stability. The second critical curve is also drawn in Fig. 4, and the insets to the curve show typical unstable beam profiles. The shape of these curves suggests an inverse power law dependence, and the theory confirms such a dependence. At and beyond the second critical curve, dynamical solutions emerge.

#### D. Anisotropic nonlocal theory

Anisotropic nonlocal theory of the space charge field, induced by the coherent CP beams in biased PR crystals, is more involved than the isotropic theory [26]. It yields significantly different results from the isotropic local model, especially when the crystal  $\hat{c}$  axis is tilted with respect to the direction of the propagation of the beams. A more complete description of CP beams requires inclusion of both the drift and the diffusion term.

In the anisotropic approximation, the NL refractive index change  $\delta n^2$  can be decomposed into the form:  $\delta n^2 = \delta n_0^2 + \delta n_m^2 [\exp(2ikz) + \exp(-2ikz)]/2$ . The modulated ( $\delta n_m^2$ ) and unmodulated ( $\delta n_0^2$ ) parts are the functions of the space charge field and the nonzero components of the electro-optic tensor. The propagation equations of the beam envelopes in the paraxial approximation are now given by:

$$i\partial_z F + \frac{1}{2}\partial_x^2 F = \delta n_0^2 F + \frac{1}{2}\delta n_m^2 B, \quad (5a)$$

$$-i\partial_z B + \frac{1}{2}\partial_x^2 B = \delta n_0^2 B + \frac{1}{2}(\delta n_m^2)^* F. \quad (5b)$$

To see the propagation behavior that is a mixture of the self-focusing and pattern formation, the counterpropagation of two wider beams in an anisotropic nonlocal medium is simulated in Fig. 5. Figures 5(a) and 5(b) show how the profiles of the beams change as they propagate. Figure 5(c) shows the profile of the forward beam as it leaves the crystal. It has split into three beams, reminiscent of the breaking of a uniform beam into stripes in the experiments on pattern formation in CP beams. The solid line in Fig. 5(d) shows the backward beam as it leaves the crystal. For comparison, the dashed line shows what the beam would look like if the nonlinearity were absent. One can see that on the one hand the backward beam gets amplified while propagating through the crystal; on the other hand the self-focusing effect of the nonlinearity is also clearly visible. The effect of the self-bending is weak, due to the short propagation distance. However, its effects are clearly visible in the asymmetry of the beam profile in Fig. 5(c).

#### E. Modulational instability

As mentioned, the configuration of two waves interacting in a NL material is one of the most used in laser physics and NL wave mixing experiments. Instabilities, self-oscillations, and chaos, which are the fundamental processes in NL optics, can be observed very often in such systems. In [1] it was demonstrated, for the first time, that self-oscillations and chaos can be obtained in an optical system without any external feedback. Authors have predicted that in the scalar approximation, CP waves interacting in a NL Kerr medium characterized by a noninstantaneous response, can undergo oscillatory and chaotic temporal evolution, above a certain input intensity threshold. When the vector nature of light is included in the theoretical consideration [4], it was found that the polarizations of CP light waves in an isotropic Kerr medium become temporally unstable, as the total intensity exceeds a certain threshold. Periodic and chaotic temporal behavior can occur in the output polarizations, as well as in the output intensities. Temporal instabilities in the polarizations of CP laser beams in atomic sodium vapor were investigated in [5]. For intensities slightly above the instability threshold, the polarizations fluctuate periodically. For higher intensities, the fluctuations become chaotic and the system evolves on a strange attractor.

Continuous-wave and oscillatory transverse instabilities were predicted for CP waves in Kerr media [11], for both the focusing and defocusing nonlinearities; neither cavity nor finite response time were required. Temporal

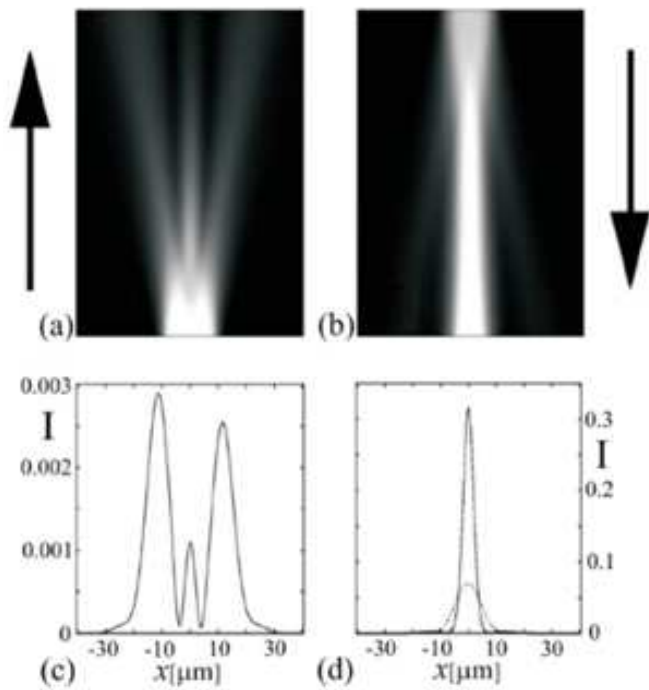


FIG. 5: Counterpropagation of two beams in a 1 mm long crystal. The crystal is tilted by  $\alpha = 10^\circ$  with respect to the propagation direction. (a) shows the evolution of the forward beam (propagating from bottom to top); (b) shows the backward beam (propagating in the opposite direction). (c) shows the profile of the forward beam as it leaves the crystal. In (d) the dashed line shows the backward beam leaving the crystal after linear propagation, whereas the solid line shows it after nonlinear propagation. Adopted from [24].

dynamics of the polarization state of CP waves in NL optical fibers was studied in [16]. It was shown that in the presence of uniform twist, the dynamics may be reduced to an integrable chiral field representation. Dynamical instabilities of CP beams in a NL two-level system were investigated numerically in [10]. When the incident intensities are increased, this system becomes unstable and exhibits complex behavior, including quasi-periodic motion and chaos. In [17] the spatial polarization instability of two intense CP laser beams in an isotropic NL dielectric fiber was investigated experimentally. It was demonstrated that the distribution of polarization states along the fiber can be identified with a polarization domain wall soliton.

Dynamical instabilities of CP self-trapped beams in PR media were reviewed in [28]. A route to chaos is described, including splitup instability, period doubling cascade, windows of intermittency, and fully developed chaos (Fig. 6). An experimental method to stabilize unstable CP solitons using photonic lattices is developed by the same group; it is presented in the section dealing with the solitons in optical lattices.

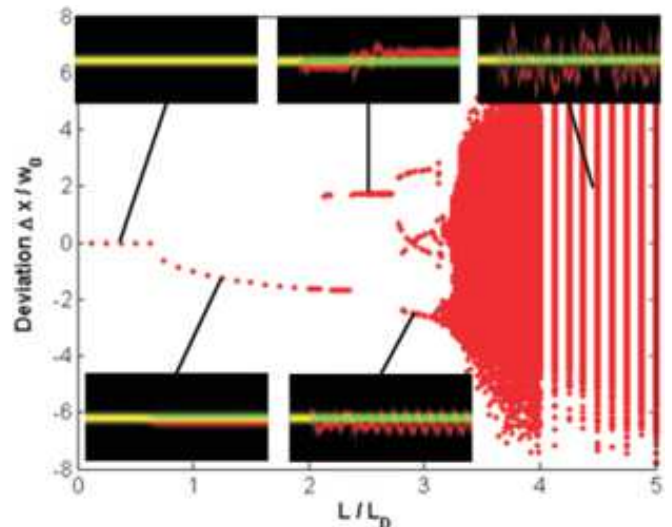


FIG. 6: Bifurcation diagram, displaying transition to chaos in a 1D model of CP self-trapped beams. Insets depict characteristic time dependence of the beams along the diagram, at one of the crystal faces. The steady beam (green) is the entering beam, the unsteady beam (red) is the exiting beam. One can note steady-state CP soliton (upper left), single splitup transition (lower left), double splitup transition (upper middle), period four oscillation (lower right), and chaotic response (upper right). Adopted from [28].

### III. TWO-DIMENSIONAL SYSTEMS

#### A. Theoretical background

Consideration of counterpropagation in two transverse dimensions in bulk media offers a more realistic and complete picture. Theoretical descriptions of CP self-trapped beams in 2D and time are provided in [25] and in [27]. The derivation of equations is similar to the 1D case [see Eqs. (1)-(4)], the major difference being the appearance of the transverse Laplacian  $\Delta_{x,y}$  in 2D equations and different boundary conditions. However, the differences in physics and results are considerable, especially if one takes into account the anisotropic nature of the PR effect in 2D. We will confine our attention here to the isotropic approximation of the system in 2D.

By assuming that the CP beams are incoherent (*i.e.*  $\varepsilon = 0$ , making the  $E_1$  term disappear), the propagation equations are given by

$$i\partial_z F + \Delta_{x,y} F = \Gamma E_0 F, \quad (6a)$$

$$-i\partial_z B + \Delta_{x,y} B = \Gamma E_0 B, \quad (6b)$$

and the temporal evolution of the system (or the time dependence of  $E_0$ ) is determined by Eq. (3a).

The most important completely new effect in 2D, in the form of dynamical spontaneous symmetry breaking, was reported for the first time in [24], where the counterpropagation of two identical numerically calculated solitary



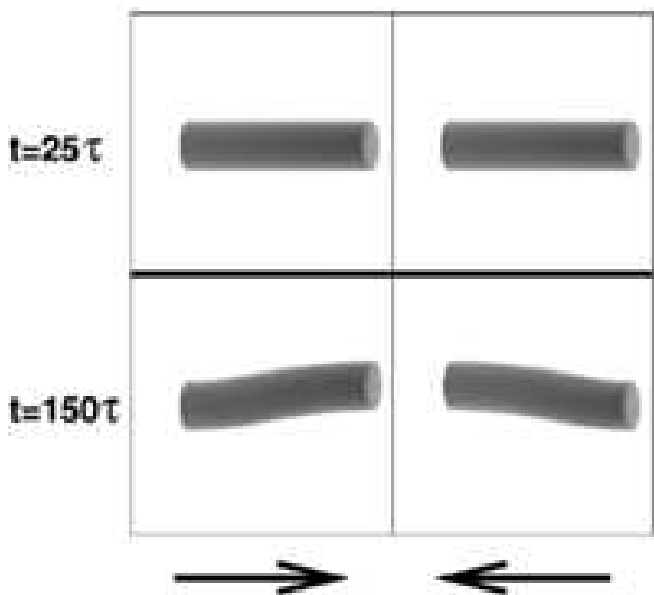


FIG. 7: CP fundamental beams for a medium of length  $L = 0.68L_D$  displaying the splitup transition. The left column shows the forward and the right column the backward beam (the arrows indicate the direction of propagation). The top row is a snapshot after  $t = 25\tau$ . Both beams propagate through the medium as solitons. At  $t = 150\tau$  (bottom row) the beams no longer propagate as steady solitons, but instead deviate on their way through the crystal. Reprinted from [26].

beam profiles was investigated. For a value of  $\Gamma \approx 14$ , corresponding to a typical experimental situation, up to the length of the medium of  $0.65L_D$  no sign of instability is observed; the beams propagate as a CP soliton. However, at  $L = 0.68L_D$  the solitary solution becomes unstable (Fig. 7). At  $t = 25\tau$  the beams still propagate as solitons through their jointly induced waveguide, but the white noise included in the system excites an eigenmode that grows in time. At  $t = 100\tau$  both beams start to deviate inside the medium from the straight initial trajectories. Since the initial problem is rotationally symmetric, the direction into which the beams deviate is random in the isotropic approximation. The intensity distribution at  $t = 150\tau$ , presented in the bottom row of Fig. 7, shows a steady state of the system. This is an example of the splitup transition in 2D. The numerical results show that the length of the medium and the power of the beams play an important role in the stability of CP solitons: decreasing/increasing the length (or the power) stabilizes/destabilizes the solitons.

These results seem to contradict the results obtained for the solitons in copropagating geometry. Two mutually incoherent solitons always attract each other, therefore one would expect that the two CP beams always form a stable soliton. This is not the case. To find an explanation of the nature and the cause of the transverse splitup instability, the CP beams were considered as particles whose motion along the  $z$  axis is subject to

the forces caused by the refractive index change in the medium. Because the medium is noninstantaneous, it was assumed that the motion of the "center of mass" of the beams is determined by the light distribution a time  $\tau$  ago. The second assumption was that the attractive force acting on the center of mass of each beam is proportional to the distance from the center of the waveguide induced in the medium by the beams. A simple harmonic oscillator-type theory of beam displacement that can account for the transverse shifts, derived in two independent ways, was presented in [24] and [27].

## B. Pattern formation and linear stability analysis

When excited beyond certain instability thresholds, very different physical systems display similar self-organized behavior that is described by the universal order parameter equations. A common necessary ingredient is the MI of spatially uniform ground state, which leads to the spontaneous formation of extended periodic spatial structures. These patterns often exhibit simple geometric structure, such as rolls, rhombi, and hexagons. Linear stability analysis (LSA) provides a threshold for the static instability in such systems.

NL optical materials are well suited for the observation of transverse MIs, especially in the CP geometry. The first complete CP pattern formation considerations and LSA in 2D was given in [29] for the counterpropagation in a Kerr medium (in 1D see [11]). It was demonstrated by a NL perturbation analysis that two very different pattern-forming modes coexist in this system. One is a hexagon-forming mode, and is dominant in the self-focusing media. The other is a roll-pattern mode, but it was found that rolls are unstable. Instead, square patterns emerge, and seem to be dominant in the self-defocusing media [29]. When the two beams are slightly frequency-detuned [14], counterpropagation in PR two-wave mixing also gives rise to the transverse MI. The patterns that develop from the initial stage of MI are found to be predominantly rolls. For induced slight misalignment, full hexagonal patterns develop.

The described phenomena are much more dependent on the geometry than on the particular form of the non-linearity. We will present here only one recent result concerning the transverse splitup instability of CP solitons (see Fig. 7). Patterns developing in wider hyper-Gaussian CP beams will be covered in Sec. 6. In the standard MI theory one follows the dynamics of weak perturbation to a wave and looks for instances of exponential growth of the perturbation. Such a growth promotes the amplification of sidebands and leads to the appearance of localized transverse structures. This approach is used much in the theory of transverse optical patterns [15]. Here however, the whole object - a CP soliton - undergoes a sudden transverse shift to a new position. Using LSA, the splitup instability is explained as a first-order phase transition, caused by the spontaneous symmetry

breaking, and the threshold curve is determined [30].

One should note that LSA is more properly applied to very broad CP beams. In the case of splitup instability, the stability analysis is applied to a low-aspect-ratio geometry, and we are aware of its limited validity. It is known in many systems with dissipative feedback that the instability of solitons and pattern forming systems follow different bifurcation routes. Here the instability of propagating solitons and the pattern formation in wide CP beams (addressed in Sec. 6) are approximately treated by the same LSA and the same threshold conditions. Qualitative agreement is found.

One starts at the steady state plane-wave solution of the system of Eqs. (3a) and (6):

$$F_0(z) = F_0(0)e^{-i\Gamma E_0 z}, \quad B_0(z) = B_0(L)e^{i\Gamma E_0(z-L)}, \quad (7)$$

where  $E_0 = -I_0/(1 + I_0)$  and  $I_0 = |F_0|^2 + |B_0|^2$ . The primary threshold is determined by the linear instability of the steady state plane-wave field amplitudes  $F_0(z)$  and  $B_0(z)$ , and the homogeneous part of the space charge field  $E_0$ . To perform LSA, a change of variables is made:

$$F = F_0(1 + f), \quad B = B_0(1 + b), \quad E = E_0(1 + e), \quad (8)$$

along with the change in the boundary conditions  $f(0) = b(L) = 0$ . Neglecting higher harmonics and terms quadratic in the perturbations  $f$ ,  $b$  and  $e$ , and following the procedure described in Ref. [14], the threshold condition is obtained in a form:

$$1 + \cos \Psi_1 \cos \Psi_2 + \left( \frac{\Psi_1}{\Psi_2} + \frac{\Psi_2}{\Psi_1} \right) \frac{\sin \Psi_1 \sin \Psi_2}{2} = 0, \quad (9)$$

where  $\Psi_1 = k^2 L$ ,  $\Psi_2 = \sqrt{k^4 L^2 - 4A\Gamma k^2 L^2}$ ,  $k$  being the transverse wavenumber. We chose  $|F_0|^2 = |B_L|^2$ , so that  $A = |F_0|^2/(1 + 2|F_0|^2)^2$ . This equation has the same form as the threshold condition in Ref. [29], except that the form and the meaning of variables  $\Psi_1$  and  $\Psi_2$  is different.

For each value of  $A$  there are two values of  $|F_0|^2$  (or  $|B_L|^2$ ) on the threshold curves represented in Fig. 8. For this reason we found it more convenient to plot the threshold intensity as a function of the square of the transverse wave vector (Fig. 9); for each pair of values of  $\Gamma$  and  $L$  then one obtains different threshold curves. Also provided in Fig. 9 are the arrows which depict how much the CP solitons jump transversely in the  $k$  space in numerical simulations, after a splitup transition. The left end of an arrow points to the peak value of  $k^2$  in the steady state, the right end points to the maximum value of the total transient change in  $k^2$ . The end points are calculated by independent numerical runs of the full simulations. For the given control parameters ( $\Gamma = 4$  and  $L = 5L_D$ ) only single or double splitup transitions are observed. It is seen that the arrows provide a qualitative

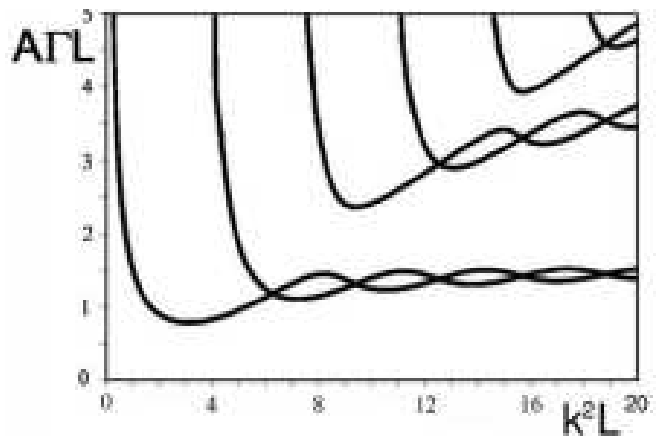


FIG. 8: Threshold curves obtained from Eq. (9). Reprinted from [30].

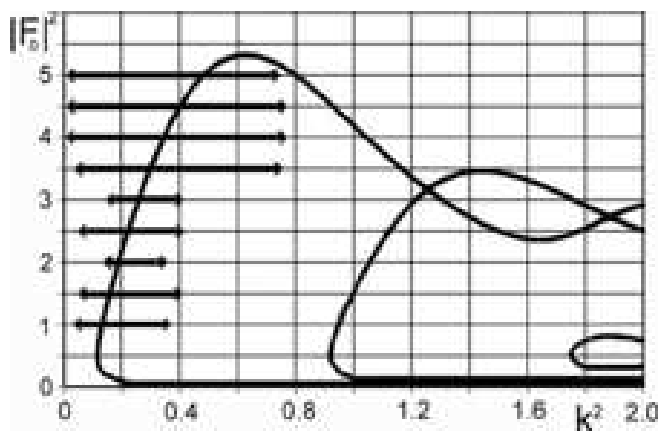


FIG. 9: Threshold intensity versus the square of the transverse wave vector  $k^2$ , for  $\Gamma = 4$  and  $L = 5L_D$ . Arrows cover the regions of jump in  $k^2$  of the solitons in the inverse space, obtained numerically. Reprinted from [30].

agreement with the form and the position of the lowest branch of the threshold curve, which signifies the first splitup transition.

## IV. EXPERIMENTAL DEMONSTRATIONS

### A. One-dimensional solitons

The first experimental observation of spatial vector solitons in the counterpropagation geometry and for coherent optical fields was reported by Cohen *et al.* [31]. The experimental setup is shown in Fig. 10. An Ar<sup>+</sup> laser beam at 488 nm is split equally into two beams, 1 and 2, that are focused to narrow stripes (15-mm FWHM) on the opposite faces, A and B, of an SBN:60 crystal (4.5 mm x 10 mm x 5 mm) in the configuration used earlier for the generation of PR screening solitons [32]. Two cameras image the two faces of the crystal. Importantly,



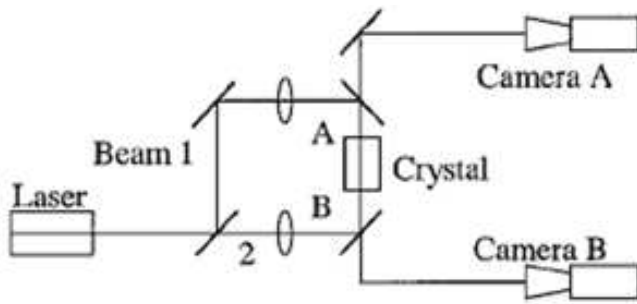


FIG. 10: Experimental setup for the generation of CP solitons [31].

the light gathered by each camera consists of both the transmitted beam and the back-reflected beam.

Figures 11(a,b) show the results of Ref. [31] for the image and intensity profiles taken by camera A at the input face B and at the output surface A, respectively, when beam 1 is blocked and the nonlinearity is off. No soliton is formed. When the two beams propagate together with the nonlinearity (with an external voltage of 900 V), the beams mutually self-trap, as shown in (c). The FWHM of this combined beam is  $15 \mu\text{m}$ , equal to the FWHM of each of the input beams at both surfaces. Thus the combined wave, consisting of both CP beams, forms a vector soliton at the specific value of the nonlinearity, determined by the applied field, the intensity ratio, and the crystal parameters (refractive index and the electro-optic coefficient). To exemplify the fact that the vector soliton is formed by both CP components, Cohen *et al.* [31] blocked beam 1 and observed the output of beam 2 without changing the voltage.

Further experimental studies of collisions between PR spatial solitons propagating in the opposite directions, performed by the same group [33], demonstrated that each of the interacting solitons significantly affects the self-bending of the other, exhibiting effective attraction for one beam and repulsion for the other. In particular, Rotschild *et al.* [33] were able to switch between coherent and incoherent interactions by introducing a piezoelectric (PZ) mirror into the experimental setup, affecting one of the optical paths. Importantly, by varying the distance between the beams, the authors did not observe noticeable changes during the coherent collision between solitons. The coherent effects that occur during the collision arise from the interference between the beams, translated into a reflection grating. Rotschild *et al.* [33] tested the presence of such a reflection grating when the solitons are truly counterpropagating, by blocking one of the beams. The existence of this grating proved the occurrence of a stable coherent interaction between the CP beams. When the PZ mirror is vibrating, the grating does not form; *i.e.*, the soliton interaction is incoherent, and no reflection is observed from the grating.

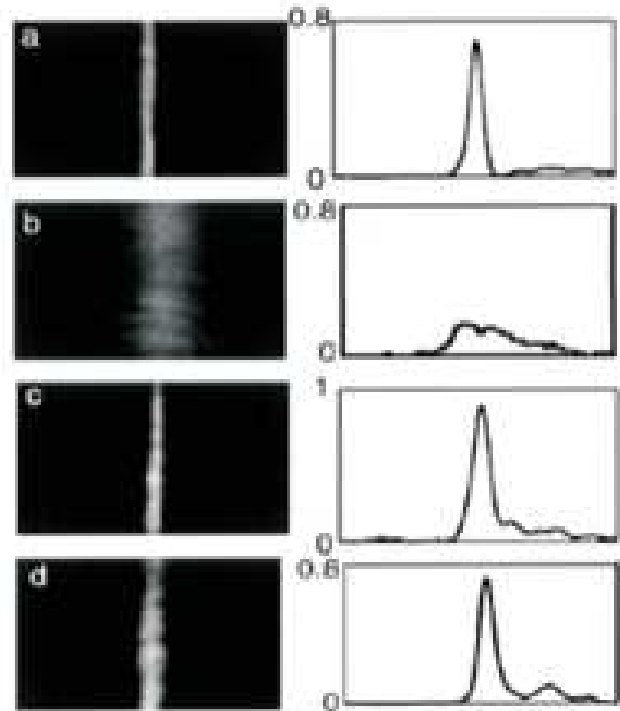


FIG. 11: Experimental images and intensity profiles taken by camera A (see Fig. 10). Intensities of beam 2 in linear medium for (a) the input and (b) the output surfaces of the crystal when beam 1 is blocked (c) Total intensity of the CP vector solitons at the left face of the crystal. (d) Intensity at the left surface when beam 1 is blocked and the nonlinearity is on (adopted from Ref. [31]).

## B. Solitons in bulk media

The first experimental study of CP solitons in a bulk medium was conducted by Jander *et al.* [34], who also observed a dynamical instability in the interaction of CP self-trapped beams in a PR medium, predicted earlier in the theoretical modeling of the time-dependent beam dynamics [23]. Jander *et al.* [34] noticed that, while the interaction of copropagating spatial optical solitons exhibits only transient dynamics and eventually results in a final steady state, the CP geometry demonstrates a dynamical instability mediated by an intrinsic feedback. Experimental observations were found to be in qualitative agreement with the numerical simulations.

Jander *et al.* [34] studied the dynamics of mutually incoherent CP solitons in cerium-doped strontium barium niobate (Ce:SBN:60) crystal, using experimental setup shown in Fig. 12. The crystal is biased by an external dc field along the transverse  $x$  direction, coinciding with the crystallographic  $c$  axis. Both beams are obtained from a single laser source and rendered mutually incoherent by a mirror oscillating with a period significantly shorter than the relaxation time constant of the PR material. Propagating in different directions, both beams individually self-focus, and the nonlinearity is adjusted

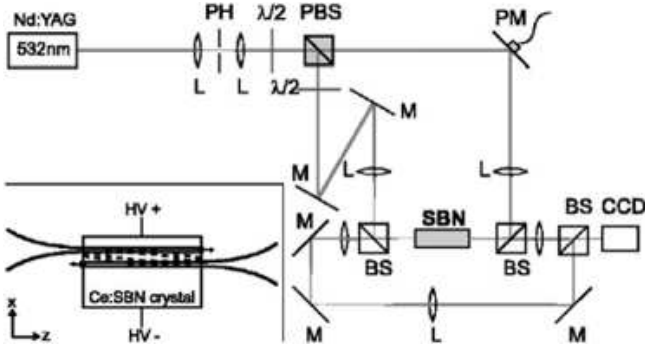


FIG. 12: Experimental setup for the study of instabilities of CP solitons [34]. Two beams are rendered mutually incoherent with an oscillating PZ mirror and focused on the opposite faces of a Ce:SBN60 crystal. Both crystal faces are imaged onto a CCD camera, allowing for synchronous observation of reflections of both the exit and input beams (Ms, mirrors; Ls, lenses; PH, pinhole; PBS, polarizing beam splitter; BS, beam splitter). Inset: CP soliton interaction in the numerical model (see details in Ref. [34]).

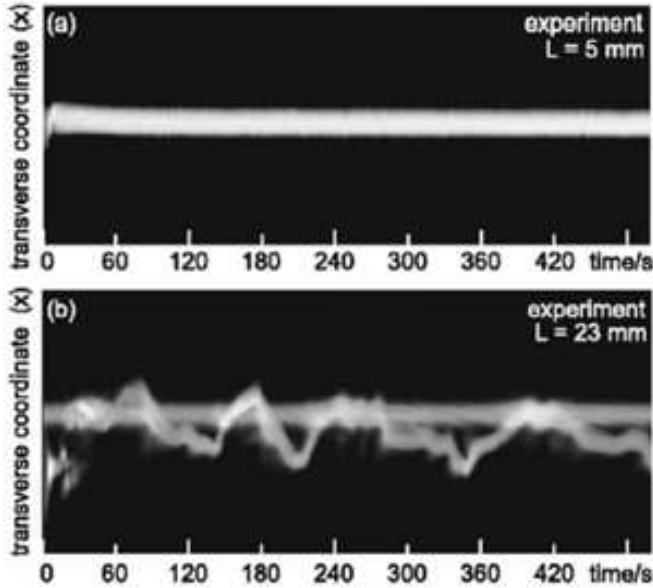


FIG. 13: Temporal plot of system dynamics. (a) Below threshold ( $L_1=5$  mm), the resulting stable and stationary state consists of two symmetrically overlapping solitons. (b) Above threshold ( $L_2=23$  mm), irregular dynamics is observed [34].

such that each of the beams individually forms a spatial soliton. To demonstrate both above and below threshold behavior with a single crystal sample, Jander *et al.* [34] utilized two medium lengths by rotating the crystal about its  $c$  axis, thus yielding  $L_1=5$  mm and  $L_2=23$  mm.

Initially, both beams are adjusted such that their inputs and outputs overlap on both ends of the crystal, if propagating independently and in a steady state, including the shift through the beam bending. This configura-

tion was chosen to minimize the possible effects of beam bending on the stability of a fully overlapping state in the form of a CP vector soliton, shown in Fig. 13(a). For comparison with the numerical simulations, experimental data are reduced to one transverse dimension: The images obtained on the exit faces of the crystal are projected onto the  $x$  axis. As these data are plotted over time, one gets a representation of the dynamics of the beam exiting the crystal face [as shown in Figs. 13(a,b)]. Changes parallel to the  $y$  axis are not represented, since most of the observable dynamics is confined to the  $x$  axis, owing to the significance of the  $c$  axis for the PR effect.

For short propagation length ( $L_1=5$  mm), the output beams on both crystal surfaces initially shift their positions, converging to an overlapping steady state, the vector soliton, see Fig. 13(a). In the case of a significantly longer medium ( $L_2=23$  mm) the beams initially self-focus separately [Fig. 13(b)] and attract and overlap. However, this state is unstable and yields to irregular repetitions of repulsion and attraction. This process does not feature any visible periodicity and is observed for time spans that are orders of magnitude longer than the time constant of the system.

More detailed experimental and numerical studies by Petrović *et al.* [30] revealed that the CP incoherent beams can form 2D spatial solitons, but they also exhibit an interesting dynamical behavior in both dimensions. Stable solitons are readily observed over the 5 mm propagation distance, with an applied field of 1.3 kV/cm and the initial beam peak intensity of about twice the background intensity. When the propagation distance is increased from 5 mm to 23 mm, for identical other conditions, a symmetry breaking transition from the stable overlapping CP solitons to unstable transversely displaced solitons is observed. The beams still self-focus approximately into solitons, but they do not overlap anymore [Figs. 14(a,b)]. At the exit face most of the beam intensity is expelled to a transversely shifted position (about 1 beam width), while a fraction of the beam remains guided by the other beam. This is another evidence of the splitup transition. At higher applied fields (stronger non-linearity) the beams start to move. The motion is such that the exiting beam rotates about or rapidly passes through the input beam, or dances irregularly around. No such long-lasting temporal changes are observed in the copropagation geometry. All these dynamical phases can qualitatively be reproduced by numerical simulation, as discussed above, in qualitative agreement with the experimental results.

The existence and stability of CP dipole-mode vector solitons in a PR medium was studied experimentally by Schröder *et al.* [35], who also investigated the transient dynamics. A dipole-mode vector soliton consists of two mutually incoherent beams: an optical dipole and a fundamental-mode beam. The individually propagating dipole does not form a spatial soliton, owing to repulsion of the dipole components. However, if a fundamental-mode beam that is incoherent to the dipole is launched

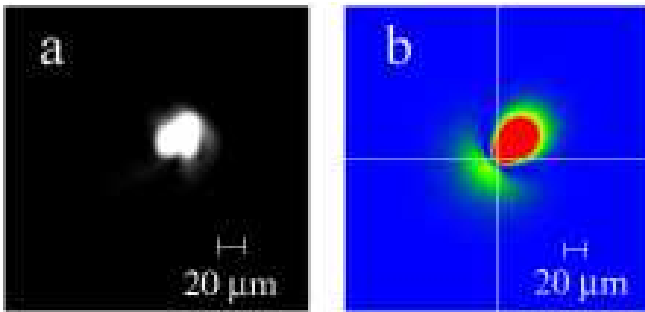


FIG. 14: Counterpropagating soliton after a splitup transition: Forward propagating component in the steady state. (a) Exit face of the crystal, experimental. (b) The corresponding numerical simulation [30].

between the dipole components, they will be trapped by means of incoherent attraction.

Schröder *et al.* [35] have proven the existence of a stable CP dipole-mode vector soliton in a PR crystal. This vector soliton differs considerably in many aspects from its counterpart in the copropagating geometry. For example, the time scale of the transient dynamics is significantly longer. During the formation the beams split, and a trapped and an untrapped part of the dipole can be observed experimentally [35].

## V. SOLITONS IN OPTICAL LATTICES

Currently, we witness an explosion of interest in the localized CP beams in photonic crystals and optically induced photonic lattices [19]. Both 1D and 2D geometries are extensively studied in a number of recent publications, and many aspects of counterpropagation are addressed. An incomplete list includes Tamm oscillations and localized surface modes at the interface between homogeneous medium and waveguide arrays; instabilities and stabilization influence of optical lattices; soliton propagation aided by reflection gratings; the behavior of CP vortices upon propagation in photonic lattices; Bloch oscillations and Zener tunneling; the questions of angular momentum transfer, conservation, and non-conservation in such systems; *etc.* In a few subsections, we will review some of these aspects.

### A. One-dimensional lattices

Interaction of CP discrete solitons in a nonlinear 1D waveguide array was investigated experimentally and numerically in [36]. Solitons of equal input powers were launched in the same channel, but propagating in the opposite directions. Similar scenario to the CP soliton propagation in bulk is observed. For small input powers the interaction between solitons is weak, and almost independent propagation in the same channel is seen.

When the input power is increased, soliton instability sets in, and for a sufficiently high value the spontaneous symmetry breaking occurs, resulting in a discrete lateral displacement of the two solitons. A further increase in power leads to the temporally irregular behavior, with fast spatial fluctuations as compared to the buildup time. Numerical modeling [36] corroborated the existence of the three different regimes: stable propagation of vector solitons at low power, instability for intermediate power levels, leading to a transverse shift of the two discrete solitons, and an irregular dynamical behavior of the two beams at high input powers.

The existence of Tamm oscillations at the interface between a homogeneous medium and a 1D NL waveguide array, with either cubic or saturable, self-focusing or self-defocusing nonlinearity, was demonstrated in [37]. Light gets trapped in the vicinity of the edge of the array, owing to the interplay between repulsion at the edge and Bragg reflection. Approximate analytical expressions for the repulsive potential are given for different types of nonlinearities. Tamm oscillations reduce to the surface Bloch oscillations, when the repulsive potential is a linearly decreasing function of the distance from the edge of the waveguide array.

The impact of an optically-induced photonic lattice on the dynamics of CP solitons in a biased PR crystal, as well as the stabilization of CP solitons by photonic lattices, were studied in [38]. Numerical results there demonstrate that an optically-induced lattice of an appropriate period and strength can suppress or even completely arrest the instability. It is found that CP solitons launched both on-site and off-site can be stabilized. The rate of decrease of temporal dynamics of CP solitons launched on-site strongly depends on the lattice strength and its period. In the case of small periodicity and high peak intensity of the lattice, spatiotemporal oscillations are observed, with characteristics dissimilar from those exhibited by CP solitons in bulk media. Experimental results [38] demonstrate that, in most cases, soliton dynamics, *i.e.* spatiotemporal oscillations, are suppressed with the increasing strength of the optical lattice. Also, the decrease in dynamics is noted experimentally for the 1D lattice whose periodicity is comparable to the beam diameter.

### B. Solitons aided by reflection gratings

The existence of linear 1D reflection grating in a NL optical medium implies periodicity along the optical propagation direction. In the presence of an intensity-dependent nonlinearity, the interference between the two CP beams produces a second longitudinal grating. Combining these effects with the standard diffractive broadening suppression, a twofold compensation mechanism can arise, allowing for the CP soliton formation. Solitons forming in a reflection grating in the presence of Kerr nonlinearity were investigated theoretically in

[39, 40, 41, 42, 43].

Bright and dark 1D solitons counterpropagating along the reflection grating were analytically investigated in [39]. It was shown that, depending on the Bragg matching between the light and the Fourier component of the grating, three different regimes of soliton existence arise. In the first regime, when the deviation from exact Bragg matching is small, both bright and dark solitons can exist. The other two regimes occur for greater deviations from the exact Bragg matching. Deviations above Bragg matching allow only bright, and deviations below Bragg matching allow only dark solitons. In the two regimes the solitons are insensitive to the mutual phase difference.

Transverse and soliton instabilities due to counterpropagation through a reflection grating in Kerr media were considered in [40]. It was shown that the presence of the grating broadens and narrows the stability region of plane waves in focusing and defocusing media, respectively. Counterpropagation of spatial optical solitons in a linear reflection grating, in the presence of a longitudinally modulated Kerr nonlinearity, was investigated in [41]. The existence of symmetric soliton pairs supported by an effective Kerr-like nonlinearity is predicted analytically. In addition, two families of solitons are introduced, in which the phase conjugation coupling exactly balances the Kerr holographic focusing. Properties of a general family of dark reflection solitons in defocusing Kerr media were considered in [42]. Two families of solitons counterpropagating along the grating direction in a modulated Kerr medium (asymmetrical one-solitons and coherent-incoherent two-solitons) were introduced in [43].

### C. Two-dimensional lattices

Self-trapped CP beams in fixed optical photonic lattices were for the first time investigated in [44]. When the propagation in photonic lattices is considered, the propagation equations are given by Eqs. (6) (assuming  $E_0 \rightarrow E$ ), and Eq. (3a) for the space charge field is modified, to include the transverse intensity distribution of the optically induced lattice array  $I_g$ :

$$\tau \partial_t E + E = -\frac{I + I_g}{1 + I + I_g}, \quad (10)$$

where  $I = |F|^2 + |B|^2$  is the total beam intensity. Spontaneous symmetry breaking of the head-on propagating Gaussian beams is observed, as well as discrete diffraction and the formation of discrete CP vector solitons. In the case of launched vortices, beam filamentation is reported, and subsequent pinning of filaments to the lattice sites [44]. Dynamical properties of mutually incoherent self-trapped CP beams in optically induced photonic lattices, for different incident beam structures and different lattice configurations, were investigated numerically in a number of papers [45, 46, 47, 48, 49, 50, 51].

#### 1. Launched vortices

Rotational properties of mutually incoherent self-trapped vortex beams in optically induced fixed finite photonic lattices with a central defect were considered numerically in [45]. The defect is introduced either by omitting a lattice site in the center, or by defining a specific defect function. An interesting example of rotation of vortex filaments in the presence of a defect in the triangular photonic lattice is presented in Fig. 15. Although it looks as if the vortex filaments are rotating only within the defect in the center of the lattice, they also rotate away from the center, by tunneling between the lattice sites. We call this tunneling the nonlocal rotation, as opposed to the local rotation within the defect. The tunneling rotation is corroborated by the fact that, for all the cases presented in Fig. 15, the angular momentum of the vortex calculated over the whole lattice is considerably greater than the angular momentum of the vortex calculated only over the central part of the lattice. Nonlocal rotation in a periodic array, such as the triangular/hexagonal photonic lattice, can exist only for some values of the propagation distance  $L$ . Lattice supports nonlocal rotation only for some values of the propagation distance, with the "period" equal to  $L_D$  (Fig. 15). For the propagation distances between these values, chaotic behavior is observed, as well as the non-propagating modes.

Rotating CP structures in the non-periodic but rotationally symmetric circular photonic lattices were discussed also in [45]. Results for the head-on counterpropagation of two centered vortices with the opposite topological charges in a circular photonic lattice, with a negative defect in the center, indicate rich dynamical behavior as a function of the control parameters  $\Gamma$  and  $L$ . For lower values of  $\Gamma$  or  $L$  stable structures are seen, in the form of well-preserved vortex core, centered at the defect, and filaments focused onto the neighboring lattice sites. Above this region stable rotating tripoles and quadrupoles exist. For higher values of the parameters irregular rotating structures and unstable structures (*i.e.* constantly changing structures of unrecognizable shape) are identified. The rotating structures with filaments pinned to the lattice sites can exist only in the presence of lattice and have no analogs in the CP vortices propagating in bulk media.

#### 2. Gaussian beams

Time-dependent rotation of CP mutually incoherent self-trapped Gaussian beams in periodic optically induced fixed photonic lattices was investigated numerically in [46, 47]. In these papers lattice arrays with the square or triangular arrangements of beams were considered, with the central lattice beam absent. Head-on CP Gaussian beams were launched into the center of the lattice, parallel to the lattice beams. For both photonic

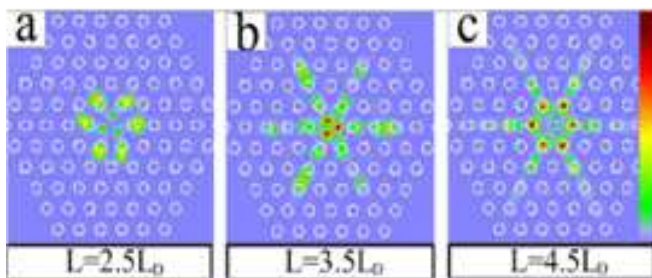


FIG. 15: Local and nonlocal rotation of vortices in triangular lattice for various propagation distances. For propagation distances between these values chaotic behavior is observed. Input vortices have the opposite topological charge  $\pm 1$ . Intensity distribution of the forward field at its output face is presented for parameters:  $\Gamma = 17$ , lattice spacing  $d = 28\mu\text{m}$ , FWHM of lattice beams  $12.7\mu\text{m}$ , input FWHM of vortices  $26.2\mu\text{m}$ , maximum lattice intensity  $I_g = 5I_d$ ,  $|F_0|^2 = |B_L|^2 = 5I_d$ . Reprinted from [45].

lattices the periodic rotation was found (see Fig. 16 for triangular lattice) in a very narrow region of control parameters. Each Gaussian beam collapses to a displaced soliton-like beam, and after transient dynamics starts to rotate indefinitely. Since for the parameters of such stable periodic solutions there exist no stable steady states, and since in numerics Eq. (10) becomes equivalent to the scalar nonlinear delay-differential equation, this phenomenon is recognized as a supercritical Hopf bifurcation. The central parts of Gaussians rotate regularly in the center of the lattice, owing to the defect, and along the whole crystal. Filaments away from the center rotate with the same frequency about the symmetry axis of the lattice, by tunneling between the lattice sites, but only close to the exit face of the crystal.

Gaussian-induced rotating structures present soliton solutions, because they preserve shape along the main symmetry direction during the rotation. The physical origin behind the nonlocal rotation is incoherent interaction and spontaneous symmetry breaking, while the rotation is realized through the tunneling. Observed rotating structures are stable in the presence of up to 5% noise added to the input beam intensity and phase. Spontaneous symmetry breaking via noise determines the direction of rotation, both directions occurring with 50% probability. For the same control parameters, CP Gaussian beams show very irregular dynamical behavior in the absence of lattice, but very stable propagation is found in the presence of lattices without defects.

### 3. Stable rotating solitons

For geometries and parameters which allow stable rotation, the existence of solitonic 2D solutions was investigated by considering Eqs. (6) and (10) in the steady state [46]. Due to their symmetry, the above equations suggest the existence of a fundamental 2D soliton solution of the

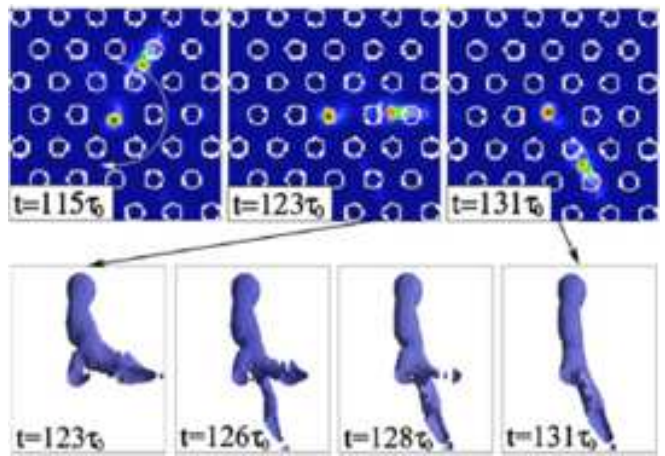


FIG. 16: Gaussian-induced rotation for the triangular photonic lattice: intensity distribution of backward beam at its exit face of the crystal, presented at different times. The second row shows isosurface plots of a rotating structure at characteristic times. Parameters:  $\Gamma = 25$ , input FWHM of CP Gaussian beams  $11\mu\text{m}$ , beam power 3.80, propagation distance  $L = 2L_D = 8\text{mm}$ , input beam intensity  $|F_0|^2 = |B_L|^2 = 1I_d$ , lattice spacing  $d = 28\mu\text{m}$ , FWHM of lattice beams  $12.7\mu\text{m}$ , and maximum lattice intensity  $I_0 = 20I_d$ . Adopted from [46].

form:

$$F = u(x, y) \cos(\theta)e^{i\mu z}, \quad B = u(x, y) \sin(\theta)e^{-i\mu z}, \quad (11)$$

where  $\mu$  is the propagation constant and  $\theta$  is an arbitrary projection angle. An appropriate choice for the CP beams is  $\theta = \pi/4$ ; the same analysis can be applied to the copropagating geometry, but with the choice  $\theta = 0$ . When this solution is substituted in Eqs. (6), they both transform into one, degenerate equation:

$$\mu u + \Delta u + \Gamma u \frac{|u|^2 + I_g}{1 + |u|^2 + I_g} = 0. \quad (12)$$

The soliton solutions of Eq. (12) can be found using the modified Petviashvili iteration method. Because of the CP geometry, these solitonic solutions are stable only up to some critical value of the propagation distance. Gaussian input beams and the same parameters as in the full numerical simulations are used in search of the stable soliton solutions. The propagation constant  $\mu$  is varied, in order to find the beam power ( $P = \int \int |u|^2 dx dy$ ) corresponding to the stable rotating structures. Figure 17 depicts the power diagram, together with the characteristic soliton solutions for the case of triangular photonic lattice; the filled circles represent the characteristic types of symmetric discrete soliton solutions. By increasing the propagation constant  $\mu$  these solutions become more localized and asymmetric. Only for the beam powers corresponding to the less localized symmetric soliton solu-



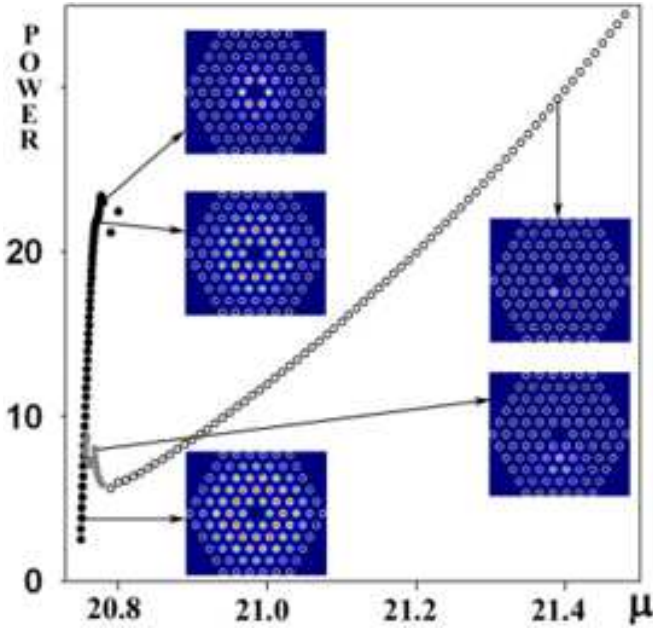


FIG. 17: Power diagram of soliton solutions for the triangular photonic lattice. Various symbols indicate different kinds of soliton solutions, characterized by the corresponding profiles. Reprinted from [46].

tions, and for the lower values of  $\mu$ , can one find Gaussian induced rotation in numerical simulations.

#### 4. Angular momentum transfer

The transfer of orbital angular momentum (AM) from vortex beams to an optically induced photonic lattice was demonstrated numerically in [51]. An optically induced photonic lattice is, in fact, a complex propagating laser beam, which means that the propagation equations for the total system of interacting incoherent CP beams in the computational domain should be of the form:

$$i\partial_z F = -\Delta F + \Gamma EF, \quad i\partial_z G_f = -\Delta G_f + \Gamma EG_f, \quad (13a)$$

$$i\partial_z B = \Delta B - \Gamma EB, \quad i\partial_z G_b = \Delta G_b - \Gamma EG_b, \quad (13b)$$

where  $G_f$  and  $G_b$  are the envelopes of the forward and backward propagating lattice beams, and  $I = |F|^2 + |B|^2$  and  $I_g = |G_f|^2 + |G_b|^2$  are the corresponding beam intensities; the temporal evolution of the space charge field is given by Eq. (10), as before.

Numerical results for the transfer of AM in the interacting CP beams are presented in Fig. 18. It was found that the transfer of orbital AM is minimal in the interacting CP lattices, and that the total AM – meaning the sum  $Lz(F) + Lz(G_f) + Lz(B) + Lz(G_b)$  of all momenta along the propagation  $z$  axis – is not conserved in this case. More precisely, the difference of AM of CP beams  $Lz(F) + Lz(G_f) - Lz(B) - Lz(G_b)$  is conserved, whereas

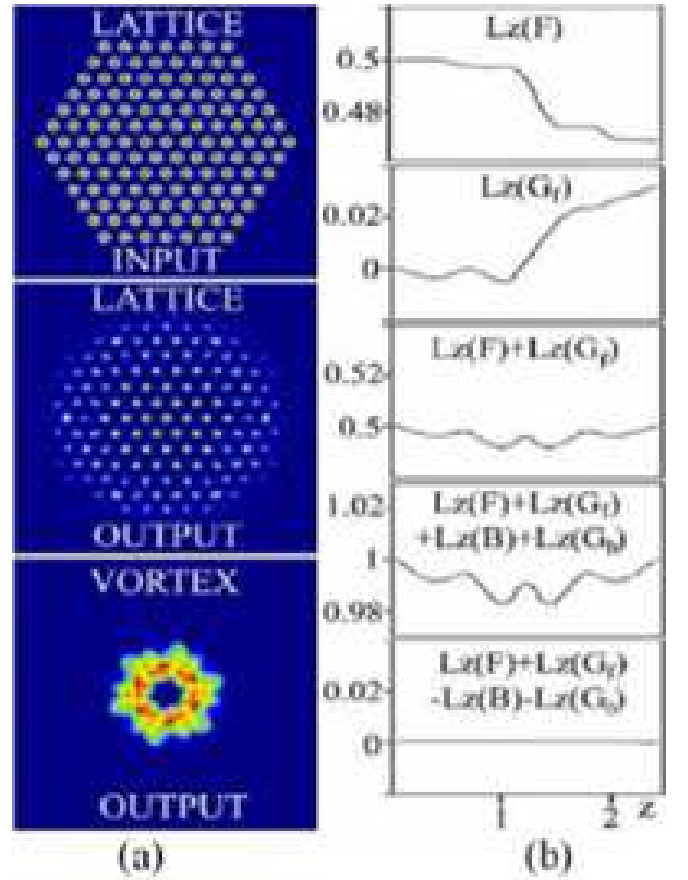


FIG. 18: Transfer of angular momentum in the interacting CP beams. (a) Forward lattice at the input and output faces, and the vortex at the output face. (b) Different normalized angular momenta. Parameters:  $\Gamma = 3$ ,  $L = 2.5L_D = 10$  mm, lattice spacing  $28\mu\text{m}$ , FWHM of input vortices  $24.6\mu\text{m}$ , FWHM of input lattice beams  $9\mu\text{m}$ , maximum input intensity  $|F_0|^2 = |B_L|^2 = 5I_d$ , and the maximum input lattice intensity  $|G_f|^2(z=0) = |G_b|^2(z=L) = 20I_d$ . Adopted from [51].

their sum is not. Even though any real optically induced photonic lattice is an interacting beam, in a number of papers it is treated approximately as a fixed lattice. It was found in [51] that the transfer of orbital AM can be substantial in the fixed periodic lattices, and that there is always a considerable loss of AM. Only in the fixed radially periodic lattices there is no problem with the conservation of AM of propagating light – it is a conserved quantity there.

Different behavior noted in the interacting and fixed lattices can rigorously be explained [51]. By using the standard definition for the  $z$  component of the orbital AM,  $Lz(F) = -\frac{i}{2} \int \int dx dy F^*(x, y)(x\partial_y - y\partial_x)F(x, y) + c.c.$ , the derivative of the difference of AM for the assumed CP geometry of propagation in the steady state is given by:

$$\frac{\partial Lz(F)}{\partial z} + \frac{\partial Lz(G_f)}{\partial z} - \frac{\partial Lz(B)}{\partial z} - \frac{\partial Lz(G_b)}{\partial z}$$



$$\begin{aligned}
&= \int_0^\infty \rho d\rho \Gamma \int_0^{2\pi} d\varphi E \frac{\partial(|F|^2 + |G_f|^2 + |B|^2 + |G_b|^2)}{\partial\varphi} \\
&= \int_0^\infty \rho d\rho \Gamma [\ln(1 + I + I_g) - I - I_g] \Big|_0^{2\pi}, \quad (14)
\end{aligned}$$

where  $\rho$  and  $\varphi$  are the cylindrical coordinates. The difference of AM is conserved in the case of interacting CP lattices, because the space charge field  $E$  is then an explicit function of  $I + I_g$ , the integration in  $\varphi$  is over a perfect derivative, and the integral in Eq. (14) is 0. However, for the fixed periodic lattices the terms involving  $G_f$  and  $G_b$  are absent, while  $E$  still contains  $I + I_g$ , and the integration in Eq. (14) is not over a perfect derivative, so the integral does not vanish. Therefore, the difference in AM is then not conserved. (Note that for the fixed radially periodic circular lattices the difference in AM is conserved.) The same Eq. (14) proves the nonconservation of the sum of AM in the general CP case: the integral then contains the difference of intensities, while  $E$  still contains the sum, so it can not be equal to 0.

#### D. Experimental demonstrations

A simple realization of a periodic NL medium is the one-dimensional system, in which the NL arrays consist of parallel, weakly coupled waveguides. In these arrays, discrete soliton interaction has been investigated for parallel beams, showing soliton attraction, repulsion, oscillatory behavior of the two beams, and soliton fusion [52, 53]. Similar to what has been observed for spatial CP solitons in bulk media, both instability of the interacting discrete solitons, leading to discrete spatial shifts, and irregular dynamical behavior for high nonlinearities can be observed in photonic lattices. Experimental results of Smirnov *et al.* [36] reveal the existence of three regimes, namely, the stable propagation of vector solitons, an instability regime leading to discrete displacements of solitons, and an irregular dynamics regime.

Figure 19 presents numerical calculations which summarize these three regimes. For a small intensity ratio the two solitons propagate stably with only weak interaction, whereas for a higher ratio instability grows and the soliton formation is partly suppressed. For even higher intensity ratio the two formed discrete solitons are displaced by one channel to the left. If the intensity ratio is further increased, no steady-state solution can be obtained anymore: The output intensity on both faces starts to fluctuate rapidly over recording times, similar to the results described in Ref. [25]. In experiment, the interaction of discrete CP solitons has been studied by Smirnov *et al.* [36] in LiNbO<sub>3</sub> waveguide array. For small input powers or intensity ratios, respectively, the interaction is weak and almost independent propagation of the two discrete solitons in the same channel is achieved. When the input power (intensity ratio) is increased, soliton instability occurs, and for sufficiently high values spontaneous

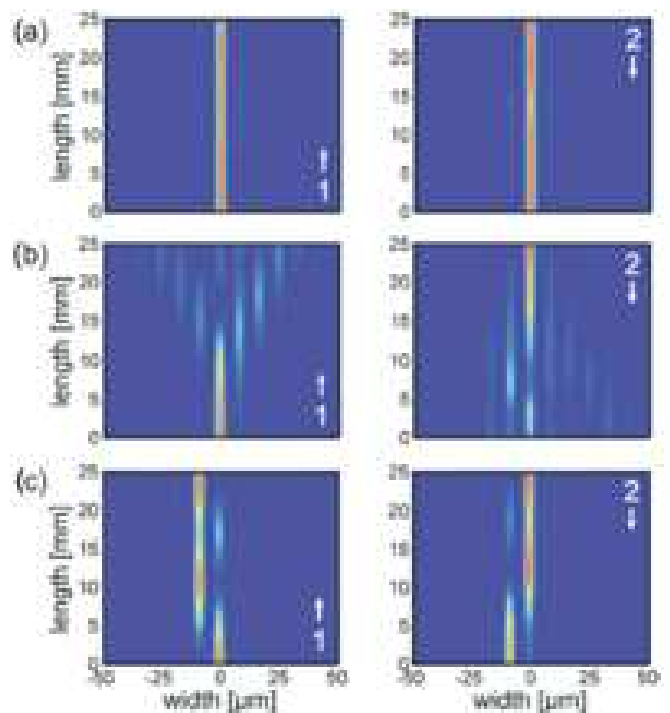


FIG. 19: Numerical simulation of the interaction of discrete CP solitons (left-hand side, beam 1; right-hand side, beam 2) for three different intensity ratios [36].

symmetry breaking with discrete lateral displacement of the two solitons is observed.

These observations led to the extension of efforts on stabilization of CP solitons in 2D volume systems by the use of 1D and 2D photonic lattices (Koke *et al.* [38]). They investigated the dependence of the instability dynamics on the period and amplitude of the lattice, and presented experimental verification for the dynamic stabilization of the bi-directional soliton states. Fig. 20 displays the arrest of instabilities of 2D CP solitons in 1D photonic lattice. It is evident that the ST oscillations are suppressed by increasing the strength of the optical lattice. This evolution is accompanied by an increased trapping of light in the neighboring lattice sites, as observed in the case of 1D CP solitons. In contrast to the 1D case, an asymmetry of trapping in the lattice channels is due to the beam-bending effect. Owing to the change in the refractive index, the self-bent soliton gets partially reflected when it passes a lattice site, and the reflected light travels along the waveguide written by the lattice wave. Moreover, the weaker oscillations in the  $y$ -direction are suppressed as the lattice peak intensity is increased. It is worth noting that the experimental stabilization of CP solitons has been achieved with lattice strengths much lower than that found in numerical simulations.

In experiments, Koke *et al.* [38] used a 2D square lattice, optically-induced in a PR crystal. They varied the lattice period and power, and monitored the positions of

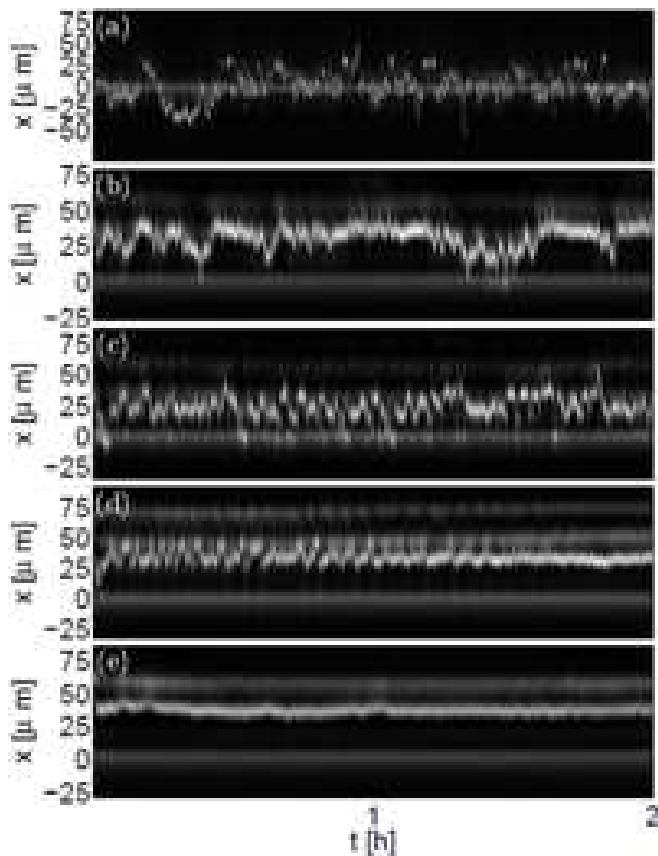


FIG. 20: Temporal evolution of the intensity distribution of 2D CP solitons in optical lattices, projected onto the  $x$ -axis (parallel to the  $c$ -axis) for different lattice powers of (a)  $250 \mu\text{W}$ , (b)  $1.0 \text{ mW}$ , (c)  $1.5 \text{ mW}$ , (d)  $2.0 \text{ mW}$ , and (e)  $2.5 \text{ mW}$ . The faint horizontal lines at  $x = 0$  mark the reflected beam at this crystal face, which acts as a reference. The results for the other crystal face show a similar behavior. Reprinted from [38].

the beams at both faces of the crystal. The inputs of the forward and backward propagating beams in their experiments have the size of  $19 \mu\text{m}$  and  $18 \mu\text{m}$ , respectively [Fig. 21(b)]. In  $10 \text{ mm}$  long crystal this corresponds to approximately 5 diffraction lengths of linear propagation. For a small lattice period ( $3 \mu\text{m}$ ) the potential induced by the lattice was too weak to arrest the instability of the CP beams. With the increased lattice period (of  $6$ ,  $9$ , and  $12 \mu\text{m}$ ) the instability was practically removed for a certain range of lattice strength. The large lattice periods, however, strongly reduce the mobility of the beams, as each beam can be fully trapped at a single lattice site. Such trapping imposes a constraint on the formation of bi-directional waveguides, which becomes sensitive on the initial alignment of the beams. Thus, beams propagating in different directions inside the crystal will not attract, as their intensity overlap will be reduced by the trapping on different lattice sites.

Without the lattice, both beams overlap weakly and their individual propagation is strongly affected by the

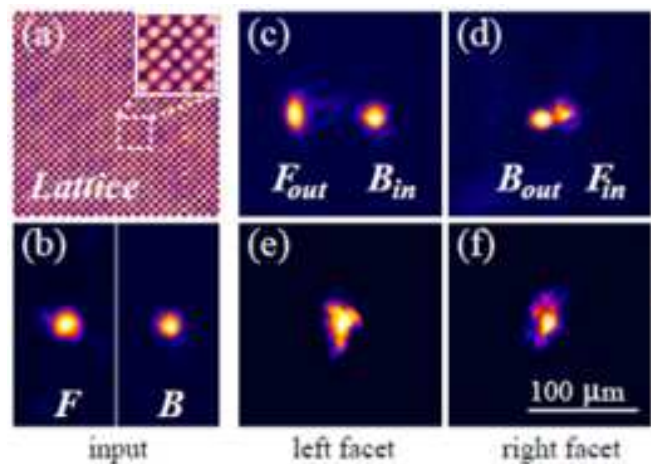


FIG. 21: Stabilization of the instability in two transverse dimensions: (a) two-dimensional square lattice of  $6 \mu\text{m}$  period. (b) Input intensity distribution for the forward (F) and the backward (B) propagating beams, respectively. (c,d) Digitally combined beam profiles at the left and right faces of the crystal, when each soliton propagates independently. (e,f) Stabilization by the lattice on both faces of the crystal, respectively [38].

beam self-focusing and self-bending. At bias electric field of  $2 \text{ kV/cm}$  and at powers of  $1 \text{ mW}$  each beam forms a spatial soliton, where the soliton size is equal to the input beam size. In Fig. 21(c,d) we show the digitally combined input and output of each beam, as they would propagate without interaction inside the crystal. When both beams co-propagate, they start to interact. After the initial attraction, the beams exhibit oscillatory dynamics.

## VI. GENERALIZATIONS

### A. Localized multipole beams

Dynamical behavior of mutually incoherent CP multipole vector solitons in an SBN:60Ce PR crystal was investigated in [54]. The dipole-dipole interaction from that paper is reproduced in Fig. 22. In the case of dipole-dipole CP solitons, two identical dipoles with the components out of phase were counterpropagated head-on. The dipoles were aligned perpendicular to the external field, which points in the horizontal direction. A transverse split-up occurred, the direction of the split-up is preferentially along the direction of the external field, and it also depends on the added noise [Fig. 22(b)]. Only in the case when some noise is added to one of the beams was it possible to observe skewed split-ups, in better agreement with the experiment. For the case with no noise [Fig. 22(c)], in the beginning oscillations were noticed along the  $y$  axis, and after a short time these oscillations were damped. Compared to the single CP soliton cases, the cases involving dipoles are more stable and the transient

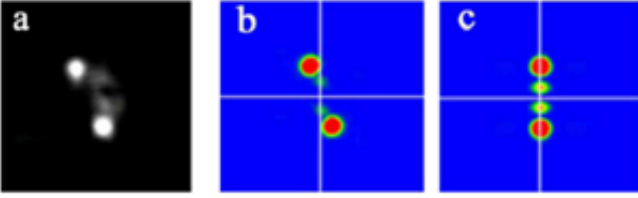


FIG. 22: Dipole-dipole interaction. (a) Experiment: the forward beam (upper) and backward beam (lower), at the exit face of the crystal. The corresponding numerical simulations of the backward beam: (b) with an extra noise of 5% added to the input beam intensity, (c) without noise. Parameters: maximum input intensity  $|F_0|^2 = |B_L|^2 = 1.3I_d$ ,  $\Gamma = 7.17$ ,  $L = 5.75L_D = 23$  mm, initial beam widths (FWHM)  $20\mu\text{m}$ , and the initial distance between the dipole partners  $40\mu\text{m}$ . Reprinted from [54].

dynamics last shorter.

The development of higher-order multipole structures and patterns in CP beams in saturable Kerr-like media was investigated in [55]. A systematic numerical study was carried out, by varying the width of beams. The results of LSA, concerning the instability of plane waves, were compared with the numerical results concerning broad hyper-Gaussian beams (used as inputs in simulations) whose width was varied. Qualitative agreement was found, due to the similarity between the plane wave and the flat-top hyper-Gaussian beam profile. We should again stress the fact that the splitup transitions do not appear to be of this common type of MI. The solitons themselves could be considered as related to the filaments of MI, and, as such, should be stable against the same kind of MI. Nonetheless, it is still of interest to explore the cross-over region by increasing the size of the solitonic beams, until they display MI. A smooth transition from the soliton splitup instabilities of narrow beams to the pattern-forming transition of broad beams is observed.

An interesting consequence of the finite size effects is the appearance of the circular saw instability, presented in Fig. 23. It appears in the form of circular saw-like rotating blades, visible in an intermediate region of beam widths, and it is caused by the MI at the edge of the beam profile. It happens very close to the absolute minimum of the control parameter  $A\Gamma L = \pi/4$  and is very robust. The rotation of optical beams along the propagation direction in saturable Kerr-like media generally appears through a bifurcation in the spatial domain. Here the bifurcation from hyper-Gaussian beams into rotating structures is due to a spatial symmetry breaking associated with a Hopf bifurcation in the time domain.

For a higher value of the control parameter  $A\Gamma L = 2$ , where one cannot expect that LSA is applicable (see Fig. 8), a more complex behavior in the form of higher-order multipole structures was found (Fig. 24). For the narrow width of incident beams, FWHM =  $20\mu\text{m}$ , a rotating displaced soliton was seen at the exiting faces of the

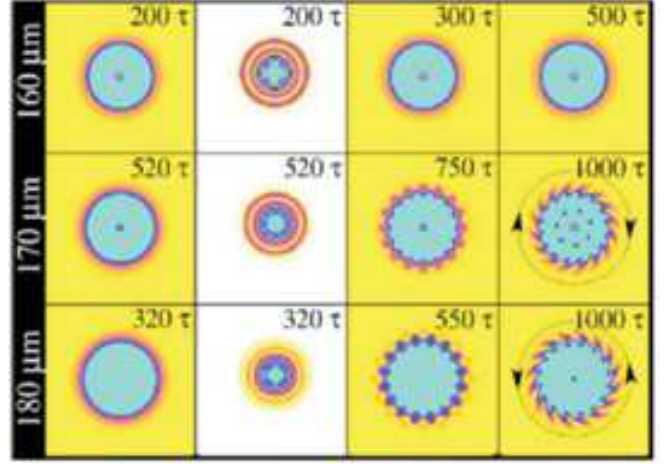


FIG. 23: Circular saw instability of the backward beam, presented in the direct and in the inverse space (the second column), for  $A\Gamma L = 0.8$  (close to the absolute minimum of the threshold curve). Transverse intensity distributions of the backward beam at the exit face are presented at different times, for three values of FWHM, recorded at the left edge of each of the rows. Circular saw-like rotating blades become visible in a region of FWHM, after a long transient development. Parameters:  $|F(0)|^2 = |B(L)|^2 = 2$ ,  $\Gamma = 6.68$ ,  $L = 1.5L_D$ . The size of the transverse window in the direct space is  $400 \times 400\mu\text{m}$ . Adopted from [55].

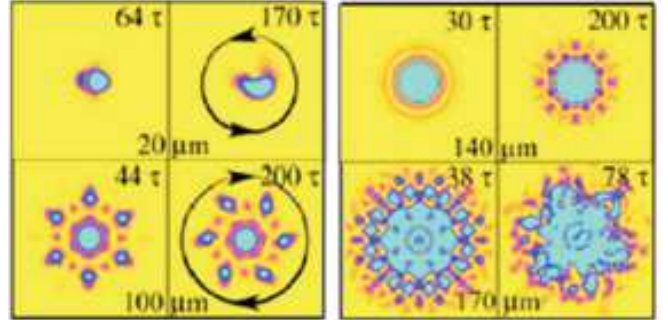


FIG. 24: Different dynamical multipole structures as the FWHM of the backward beam is increased, presented at two instances, for the control parameter  $A\Gamma L = 2$ . The figure should be viewed as a two-column picture. Parameters:  $|F(0)|^2 = |B(L)|^2 = 3$ ,  $\Gamma = 10.9$ ,  $L = 3L_D$ . The size of the transverse window is  $360 \times 360\mu\text{m}$ . Adopted from [55].

crystal, after a split-up transition. At a larger width (FWHM =  $100\mu\text{m}$ ) a hexagonal structure was observed in the beginning, which was followed by a regular rotation of filaments. Since for the parameters of such stable periodic solution there exist no stable steady state, and since numerically Eq. (3a) is equivalent to a scalar nonlinear delay-differential equation, this phenomenon is recognized as the supercritical Hopf bifurcation. For FWHM =  $140\mu\text{m}$ , steady octagonal structure appeared. For the next FWHM, after a set of various regular patterns, irregular structures took place. It should be mentioned

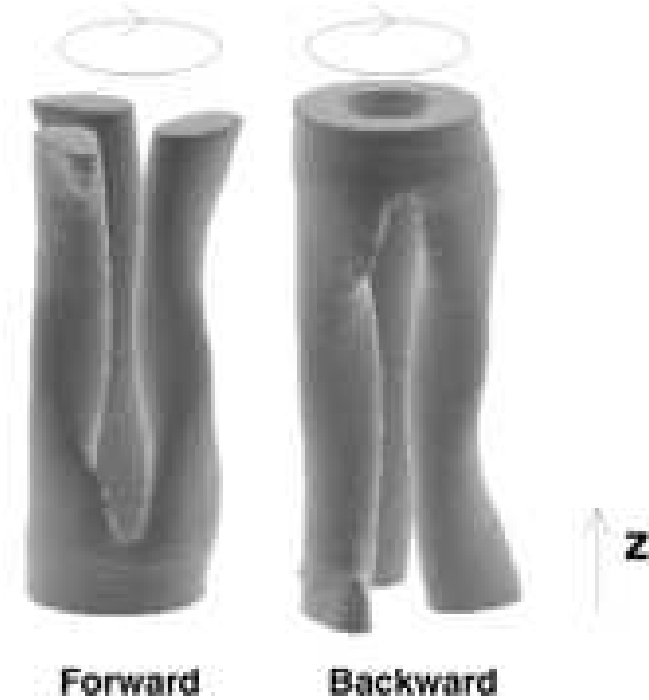


FIG. 25: Iso-surface plots of two CP vortices, with charges  $\pm 1$ . Upon collision the vortices break into three beamlets, which co-rotate continually in the sense indicated by the arrows. Adopted from [24].

that all of these structures appear after a prolonged temporal development, when the secondary instabilities set in and the interaction of NL modes takes place.

### B. Vortex beams

Colliding vortices with opposite topological charges were considered in [25]. In this case the beams break up, generally into more than two filaments. In Fig. 25 the case of two CP counter-rotating vortices is displayed, which break into three beamlets with phase shifts of  $2\pi/3$ . After a while the beams form stable rotating structures that do not change in time. When viewed in their exit faces, the beams form true rotating propellers. Such stable rotating state is interesting for developing transverse MIs over a fraction of diffraction length, even though it is generated in an isotropic model. Previously observed isotropic vortex vector solitons, with co-propagating components, tended to propagate for tens of diffraction lengths before developing MIs.

Optical CP vortices in PR crystals were investigated numerically in [56]. A general conclusion of numerical studies there was that the CP vortices in a PR medium cannot form stable CP vortex (*i.e.* ring-like) structures, propagating indefinitely. For smaller values of  $\Gamma$  or the propagation distance  $L$  stable CP vortices were observed. Nevertheless, when they break, they form very different stable filamented structures in propagating over fi-

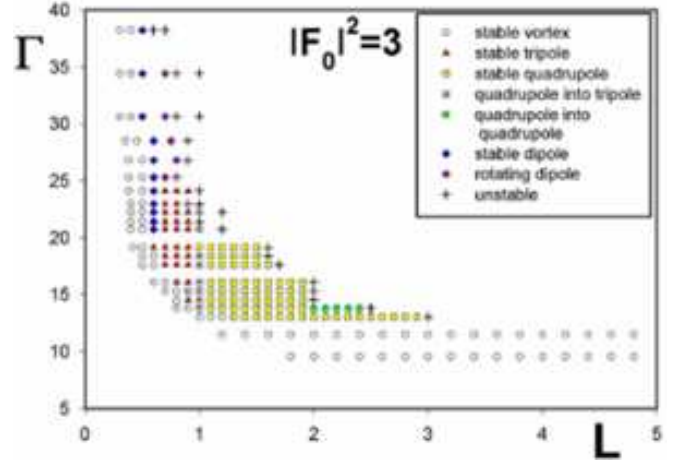


FIG. 26: Typical behavior of CP vortices in the parameter plane. The input vortices have the same topological charge  $+1$ , and maximum input intensities  $|F_0|^2 = |B_L|^2 = 3$ . Insets list the possible outcomes from vortex collisions. Reprinted from [56].

nite distances, corresponding to typical PR crystal thicknesses, which are of the order of few  $L_D$ . Numerical studies showed that the CP vortices with the same topological charge tend to form standing waves, whereas the vortices with the opposite charges tend to form rotating structures. Some typical examples of collisions between single head-on input vortices with the same topological charge  $+1$  are shown in Fig. 26, which represents the phase diagram in the plane of control parameters. One can notice in the figure a narrow threshold region which separates the stable vortices from the other structures. The shape of the threshold region follows the general  $\Gamma L = \text{const.}$  form. Above this region stable dipoles, tripoles and quadrupoles are seen, in the form of standing waves. For higher values of the parameters, the following quasi-stable situations are identified: the transformation of a quasi-stable quadrupole into a stable tripole, several transformations of quadrupoles into quadrupoles, and a stable rotating dipole. Above the quasi-stable region, CP vortices produced unstable structures.

### C. Counterpropagating beams in liquid crystals

Nematic liquid crystals (NLC) exhibit huge optical nonlinearities, owing to large refractive index anisotropy, coupled with the optically-induced collective molecular reorientation. They behave in a fluid-like fashion, but display a long-range order that is characteristic of crystals. Thanks to the optically nonlinear, saturable, non-local and nonresonant response, NLC have been the subject of considerable study in recent years. The behavior of CP self-focused beams in bulk NLC, both in time and in three spatial dimensions was investigated in [57, 58], using an appropriately developed theoretical model and



a numerical procedure based on the beam propagation method.

The evolution of slowly-varying beam envelopes  $F$  and  $B$ , linearly polarized along  $x$  axis and propagating along  $z$  axis in a NLC cell, is described by the following paraxial wave equations:

$$2ik \frac{\partial F}{\partial z} + \Delta F + k_0^2 \varepsilon_a [\sin^2 \theta - \sin^2(\theta_{\text{rest}})] F = 0, \quad (15a)$$

$$-2ik \frac{\partial B}{\partial z} + \Delta B + k_0^2 \varepsilon_a [\sin^2 \theta - \sin^2(\theta_{\text{rest}})] B = 0, \quad (15b)$$

where  $F$  and  $B$  are the forward and backward propagating beam envelopes,  $k = k_0 n_0$  is the wave vector in the medium,  $\varepsilon_a = n_e^2 - n_0^2$  is the birefringence of the medium, and  $\Delta$  is transverse Laplacian. The rest distribution angle  $\theta_{\text{rest}}$  in the presence of a low-frequency electric field is modeled by:

$$\theta_{\text{rest}}(z, V) = \theta_0(V) + [\theta_{\text{in}} - \theta_0(V)] \cdot [\exp(-z/\bar{z}) + \exp(-(L-z)/\bar{z})], \quad (16)$$

with  $\theta_0(V)$  being the orientation distribution due to the applied voltage far from the input interface.  $\theta_{\text{in}}$  is the director orientation at the boundaries  $z = 0$  and  $z = L$ , where  $L$  is the propagation distance and  $\bar{z}$  is the relaxation distance. The temporal evolution of the angle of reorientation is given by the diffusion equation:

$$\gamma \frac{\partial \theta}{\partial t} = K \Delta_{x,y} \theta + \frac{1}{4} \varepsilon_0 \varepsilon_a \sin(2\theta) [|F|^2 + |B|^2], \quad (17)$$

where  $\gamma$  is the viscous coefficient and  $K$  is Frank's elastic constant. Here  $\theta$  is the overall tilt angle, owing to both the light and the voltage influence.

It was found numerically [57, 58] that the stable vector solitons can only exist in a narrow threshold region of control parameters. Below this region the beams diffract, above they self-focus into a series of focal spots. Spatiotemporal instabilities were observed as the input intensity, the propagation distance, and the birefringence were increased. The effect of the input intensity variation on the CP Gaussian beam propagation is presented in Fig. 27. For smaller intensities [Fig. 27(a)] self-focusing is too weak to keep the beam tightly focused, so it can not pass through unchanged, as a spatial soliton. By increasing the beam intensity [Fig. 27(b)] at one point stable soliton propagation is achieved. For still higher intensities transverse motion of the beam is observed, in the form of one [Fig. 27(c)], or two consecutive jumps, resembling beam undulations. For further increase of the intensity unstable dynamical behavior of beams [Fig. 27(d)] is seen.

An interesting experimental account on the interaction of CP solitons in a NLC E7 cell is provided in [59]. Experiments are performed to estimate the nonlocality of

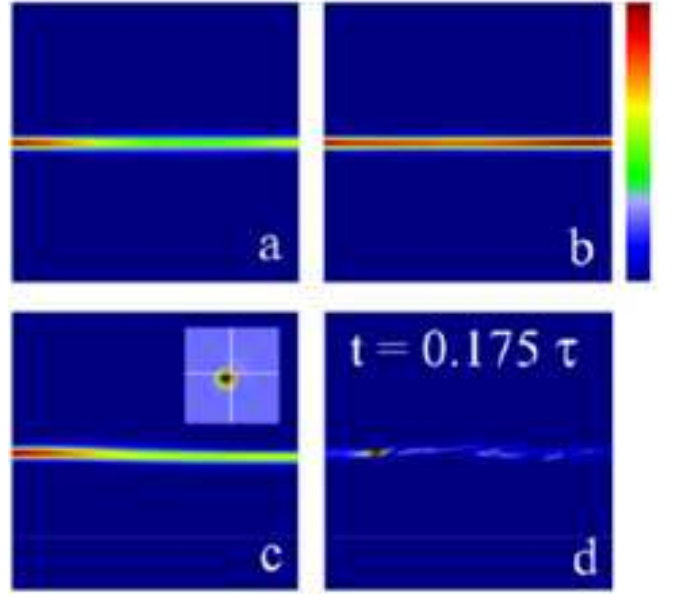


FIG. 27: Beam propagation, shown for one beam in the  $(y, z)$  plane, for different input intensities: (a)  $I = 6 \times 10^9 V^2/m^2$ , (b)  $I = 7 \times 10^9 V^2/m^2$ , (c)  $I = 8 \times 10^9 V^2/m^2$ , and (d)  $I = 9 \times 10^{10} V^2/m^2$ . In (c) the beam intensity is also shown in the  $(x, y)$  output plane. Parameters: input beam width (FWHM)  $4 \mu\text{m}$ ,  $L = 0.5 \text{ mm}$ , and  $\varepsilon_a = 0.5$ . Adopted from [58].

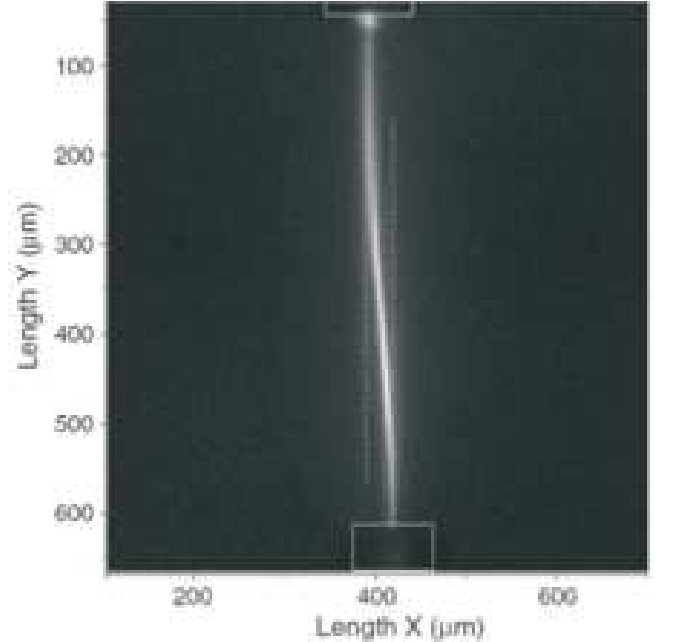


FIG. 28: Curved beam resulting from the fusion of two nonlocal CP solitons. The fibres are artificially marked, the dashed lines indicate the initial direction of the solitons. Reprinted from [59].

the reorientational nonlinearity in thick samples. The attraction of spatial optical solitons counterpropagating parallel to each other and at different small distances is displayed. An experimental method to estimate the width of the refractive index profile in a NLC sample excited by a narrow laser beam is developed. It is shown that the width of the index profile can nicely be fitted by a Lorentzian curve. A rare experimental picture of a stable CP soliton pair, launched with a considerable transverse displacement in a NLC, is presented in Fig. 28.

## VII. CONCLUSIONS

We have summarized recent developments in the physics of CP optical beams and spatial solitons, propagating in NL media. We have analyzed the formation of various stationary modes, as well as spatiotemporal instabilities of CP beams. We have employed several models for describing the evolution and interactions of optical

beams and spatial solitons that propagate in opposite directions, but the majority of the results are presented for the model of saturable PR nonlinearity. We have discussed the recent experimental observations of the counterpropagation effects and instabilities in waveguides and bulk geometries, as well as for one- and two-dimensional photonic lattices. We have also discussed several generalizations of this concept, including the CP beams of complex structures, such as multipole beams and optical vortices, as well as counterpropagation in other media, such as photonic and nematic liquid crystals.

## ACKNOWLEDGEMENT

The authors thank D. Arsenović, A. Desyatnikov, Ph. Jander, R. Jovanović, D. Jović, F. Kaiser, S. Koke, W. Krolikowski, K. Motzek, S. Prvanović, T. Richter, J. Schröder, M. Schwab, A. Strinić, and D. Träger for useful collaborations on the topics outlined in this review paper. This work has been supported by the Ministry of Science of the Republic of Serbia, under the project OI 141031, and by the Qatar National Research Foundation project NPRP25-6-7-2.

- 
- [1] Y. Silberberg and I. Bar Joseph, *Phys. Rev. Lett.* **48**, 1541 (1982).
- [2] K. Ikeda, *Opt. Commun.* **30**, 257 (1979).
- [3] K. Ikeda, H. Daido, and O. Akimono, *Phys. Rev. Lett.* **46**, 709 (1980).
- [4] A.L. Gaeta, R.W. Boyd, J.R. Ackerhalt, and P.W. Milonni, *Phys. Rev. Lett.* **58**, 2432 (1987).
- [5] D.J. Gauthier, M.S. Malcuit, and R.W. Boyd, *Phys. Rev. Lett.* **61**, 1827 (1988).
- [6] W.J. Firth, *J. Mod. Opt.* **37**, 151 (1990).
- [7] T. Ackemann and W. Lange, *Appl. Phys. B* **72**, 21 (2001).
- [8] R. Neubecker, G.-L. Oppo, B. Thüring, and T. Tschudi, *Phys. Rev. A* **52**, 791 (1995).
- [9] T. Honda, H. Matsumoto, M. Sedlatschek, C. Denz, and T. Tschudi, *Opt. Commun.* **133**, 293 (1997).
- [10] R. Chang and P. Meystre, *Phys. Rev. A* **44**, 3188 (1991).
- [11] W.J. Firth and C. Paré, *Opt. Lett.* **13**, 1096 (1988).
- [12] O. Kamps, Ph. Jander, and C. Denz, *Phys. Rev. E* **72**, 016215 (2005).
- [13] C. Denz, M. Schwab, M. Sedlatschek, T. Tschudi, T. Honda, *J. Opt. Soc. Am. B* **15**, 2057 (1998).
- [14] M. Schwab, C. Denz, and M. Saffman, *Appl. Phys. B* **69**, 429 (1999); *idem*, *J. Opt. Soc. Am. B* **18**, 628 (2001).
- [15] C. Denz, M. Schwab, and C. Weillnau, *Transverse pattern formation in photorefractive optics* (Springer, Berlin, 2003).
- [16] A.V. Mikhailov and S. Wabnitz, *Opt. Lett.* **15**, 1055 (1990).
- [17] S. Pitois, G. Millot, and S. Wabnitz, *Phys. Rev. Lett.* **81**, 1409 (1998).
- [18] W.J. Firth and C.O. Weiss, *Opt. Phot. News* **13**, 54 (2002).
- [19] Yu.S. Kivshar and G.P. Agrawal, *Optical Solitons: From Fibers to Photonic Crystals* (Academic, San Diego, 2003).
- [20] G.I. Stegman and M. Segev, *Science* **286**, 1518 (1999).
- [21] O. Cohen, R. Uzdin, T. Carmon, J.W. Fleischer, M. Segev, and S. Odulov, *Phys. Rev. Lett.* **89**, 133901 (2002).
- [22] M. Haelterman, A.P. Sheppard, and A.W. Snyder, *Opt. Commun.* **103**, 145 (1993).
- [23] M. Belić, Ph. Jander, A. Strinić, A. Desyatnikov, and C. Denz, *Phys. Rev. E* **68**, 025601(R) (2003).
- [24] K. Motzek, Ph. Jander, A. Desyatnikov, M. Belić, C. Denz, and F. Kaiser, *Phys. Rev. E* **68**, 066611 (2003).
- [25] M. Belić, Ph. Jander, K. Motzek, A. Desyatnikov, D. Jović, A. Strinić, M. Petrović, C. Denz, and F. Kaiser, *J. Opt. B* **6**, S190 (2004).
- [26] K. Motzek, M. Belić, T. Richter, C. Denz, A. Desyatnikov, Ph. Jander, and F. Kaiser, *Phys. Rev. E* **71**, 016610 (2005).
- [27] M. Belić, M. Petrović, D. Jović, A. Strinić, D. Arsenović, K. Motzek, F. Kaiser, Ph. Jander, C. Denz, M. Tlidi, and P. Mandel, *Opt. Express* **12**, 708 (2004).
- [28] Ph. Jander, J. Schröder, T. Richter, K. Motzek, F. Kaiser, M. Belić, and C. Denz, *Proc. SPIE* **6255**, 62550A (2006).
- [29] J.B. Geddes, R.A. Indik, J.V. Moloney, and W.J. Firth, *Phys. Rev. A* **50**, 3471 (1994).
- [30] M. Petrović, D. Jović, M. Belić, J. Schröder, Ph. Jander, and C. Denz, *Phys. Rev. Lett.* **95**, 053901 (2005).
- [31] O. Cohen, S. Lan, T. Carmon, J.A. Giordmaine, and M. Segev, *Opt. Lett.* **27**, 2013 (2002).
- [32] M. Shih, M. Segev, G. C. Valley, G. Salamo, B. Crosignani and P. DiPorto, *Elect. Lett.* **31**, 826 (1995).
- [33] C. Rotschild, O. Cohen, O. Manela, T. Carmon, and M. Segev, *J. Opt. Soc. Am. B* **21**, 1354 (2004).
- [34] Ph. Jander, J. Schröder, C. Denz, M. Petrović, and M. Belić, *Opt. Lett.* **30**, 750 (2005).
- [35] J. Schröder, Ph. Jander, C. Denz, T. Richter, K. Motzek, and F. Kaiser, *Opt. Lett.* **30**, 1042 (2005).
- [36] E. Smirnov, M. Stepić, C.E. Rüter, V. Shandarov, and



- D. Kip, *Opt. Lett.* **32**, 512 (2007).
- [37] M. Stepić, E. Smirnov, C.E. Rüter, D. Kip, A. Maluckov, and Lj. Hadžievski, *Opt. Lett.* **32**, 823 (2007).
- [38] S. Koke, D. Träger, Ph. Jander, M. Chen, D.N. Neshev, W. Krolikowski, Yu.S. Kivshar, and C. Denz, *Opt. Express* **15**, 6279 (2007).
- [39] A. Ciattoni, C. Rizza, E. DelRe, and E. Palange, *Opt. Lett.* **31**, 1507 (2006).
- [40] C. Rizza, A. Ciattoni, E. DelRe, and E. Palange, *Opt. Lett.* **31**, 2900 (2006).
- [41] A. Ciattoni, C. Rizza, E. DelRe, and E. Palange, *Phys. Rev. Lett.* **98**, 043901 (2007).
- [42] C. Rizza, A. Ciattoni, E. DelRe, and E. Palange, *Phys. Rev. A* **75**, 063824 (2007).
- [43] C. Rizza, A. Ciattoni, and E. DelRe, *Phys. Rev. A* **78**, 013814 (2008).
- [44] M. Belić, D. Jović, S. Prvanović, D. Arsenović, and M. Petrović, *Opt. Express* **14**, 794 (2006).
- [45] M.S. Petrović, *Opt. Express* **14**, 9415 (2006).
- [46] D.M. Jović, S. Prvanović, R.D. Jovanović, and M.S. Petrović, *Opt. Lett.* **32**, 1857 (2007).
- [47] D. Jović, S. Prvanović, R. Jovanović, and M. Petrović, *Acta Physica Polonica A* **112**, 1067 (2007).
- [48] D. Jović, R. Jovanović, S. Prvanović, M. Petrović, and M. Belić, *Optical Materials* **30**, 1173 (2008).
- [49] M. Belić, M. Petrović, D. Jović, A. Strinić, D. Arsenović, S. Prvanović, R. Jovanović, and N. Petrović, *Acta Physica Polonica A* **112**, 729 (2007).
- [50] M. Belić, M. Petrović, D. Jović, A. Strinić, D. Arsenović, S. Prvanović, and N. Petrović, *Asian J. Phys* **15**, 283 (2006).
- [51] M.S. Petrović, D.M. Jović, M.R. Belić, and S. Prvanović, *Phys. Rev. A* **76**, 023820 (2007).
- [52] H. Meng, G. Salamo, M. Shih, and M. Segev, *Opt. Lett.* **22**, 448 (1997).
- [53] D. Kip, M. Wesner, C. Herden, and V. Shandarov, *Appl. Phys.* **B68**, 971 (1999).
- [54] D. Jović, M. Petrović, M. Belić, J. Schröder, Ph. Jander, and C. Denz, *Opt. Express* **13**, 10717 (2005).
- [55] D. Jović, M. Petrović, and M. Belić, *Opt. Commun.* **281**, 2291 (2008).
- [56] D. Jović, D. Arsenović, A. Strinić, M. Belić, and M. Petrović, *Opt. Express* **13**, 4379 (2005).
- [57] A.I. Strinić, D.M. Jović, M.S. Petrović, D.V. Timotijević, N.B. Aleksić, and M.R. Belić, *Opt. Express* **14**, 12310 (2006).
- [58] A.I. Strinić, D.M. Jović, M.S. Petrović, D.V. Timotijević, N.B. Aleksić, and M.R. Belić, *Optical Materials* **30**, 1213 (2008).
- [59] J.F. Henninot, J.F. Blach, and M. Warengem, *J. Opt. A* **9**, 20 (2007).